Received: 7 February 2024 | Revised: 29 April 2024 | Accepted: 1 May 2024

DOI: 10.1111/gcb.17320

Global Change Biology WILEY

RESEARCH ARTICLE

Controls and relationships of soil organic carbon abundance and persistence vary across pedo-climatic regions

Sophie F. von Fromm[1,2] | Alison M. Hoyt[3] | Carlos A. Sierra[1] | Katerina Georgiou[4] | Sebastian Doetterl[2] | Susan E. Trumbore[1]

[1]Department of Biogeochemical Processes, Max-Planck-Institute for Biogeochemistry, Jena, Germany

[2]Department of Environmental Science, ETH Zurich, Zurich, Switzerland

[3]Department of Earth System Science, Stanford University, Stanford, California, USA

[4]Physical and Life Sciences Directorate, Lawrence Livermore National Laboratory, Livermore, California, USA

Correspondence
Sophie F. von Fromm, Department of Biogeochemical Processes, Max-Planck-Institute for Biogeochemistry, Jena, Germany.
Email: sfromm@dartmouth.edu

Present address
Sophie F. von Fromm, Now at Dartmouth College, Hanover, New Hampshire, USA

Funding information
International Max Planck Research School for Global Biogeochemical Cycles (IMPRS-gBGC); H2020 European Research Council, Grant/Award Number: 695101

Abstract

One of the largest uncertainties in the terrestrial carbon cycle is the timing and magnitude of soil organic carbon (SOC) response to climate and vegetation change. This uncertainty prevents models from adequately capturing SOC dynamics and challenges the assessment of management and climate change effects on soils. Reducing these uncertainties requires simultaneous investigation of factors controlling the amount (SOC abundance) and duration (SOC persistence) of stored C. We present a global synthesis of SOC and radiocarbon profiles ($n_{Profile}$ = 597) to assess the timescales of SOC storage. We use a combination of statistical and depth-resolved compartment models to explore key factors controlling the relationships between SOC abundance and persistence across pedo-climatic regions and with soil depth. This allows us to better understand (i) how SOC abundance and persistence covary across pedo-climatic regions and (ii) how the depth dependence of SOC dynamics relates to climatic and mineralogical controls on SOC abundance and persistence. We show that SOC abundance and persistence are differently related; the controls on these relationships differ substantially between major pedo-climatic regions and soil depth. For example, large amounts of persistent SOC can reflect climatic constraints on soils (e.g., in tundra/polar regions) or mineral absorption, reflected in slower decomposition and vertical transport rates. In contrast, lower SOC abundance can be found with lower SOC persistence (e.g., in highly weathered tropical soils) or higher SOC persistence (e.g., in drier and less productive regions). We relate variable patterns of SOC abundance and persistence to differences in the processes constraining plant C input, microbial decomposition, vertical C transport and mineral SOC stabilization potential. This process-oriented grouping of SOC abundance and persistence provides a valuable benchmark for global C models, highlighting that pedo-climatic boundary conditions are crucial for predicting the effects of climate change and soil management on future C abundance and persistence.

KEYWORDS
climate, mass-preserving spline, model benchmarking, one-pool model, radiocarbon, soil mineralogy, tropical soils, two-pool model

1 | INTRODUCTION

The timescales and magnitudes of soil organic carbon (SOC) responses to climate and vegetation change are among the largest uncertainties in the terrestrial C cycle. A substantial fraction of these uncertainties relates to the persistence and cycling of C in soils across scales and depths (Wieder et al., 2018). Modeling radiocarbon measurements ($\Delta^{14}C$) provides insights into the average time a C atom remains in the soil, reflecting SOC persistence, which needs to be linked to SOC abundance to better understand potential interactions between the timescale and magnitude of SOC responses to change. However, most large-scale studies of SOC dynamics have mainly focused on either the drivers of SOC abundance (e.g., Doetterl et al., 2015; Luo et al., 2021; Quesada et al., 2020; Rasmussen et al., 2018; von Fromm et al., 2021; Yu et al., 2021) or SOC persistence (e.g., Chen et al., 2021; He et al., 2016; Mathieu et al., 2015; Shi et al., 2020; von Fromm et al., 2023). Only a few studies have addressed them together; these studies found that the controls and relationship between SOC abundance and persistence at the continental scale are not necessarily identical (Heckman et al., 2021, 2023). Thus, assessing soil responses to changes in vegetation and climate and informing C modeling efforts across scales require a better understanding of the patterns and controls of both SOC abundance and persistence across regions and with soil depth.

Both measures, SOC abundance and persistence, have in common that they are the result of what remains from past soil C inputs. Therefore, their variation with depth depends on incoming C fluxes, transport, bio-transformations, and the duration of C protection prior to release from the soil (Basile-Doelsch et al., 2020). Carbon inputs at a given soil depth include plant litter (above- or belowground), bioturbation, and vertical transport of dissolved organic carbon (DOC) from one soil layer to another, while losses of SOC are the result of mineralization, erosion, and leaching of DOC. Microbial decomposition results in both mineralization and biotransformation of SOC, with the potential for aging of C by being recycled internally within the microbial community. Other interactions slowing or preventing SOC from being decomposed include organo-mineral interactions, with the strength of those interactions related to the persistence of SOC over varying amounts of time (years to millennia; Oades, 1988; Baldock & Skjemstad, 2000). Important mineral groups involved in the formation of strong organo-mineral bonds and interactions with SOC include poorly crystalline metal phases and 2:1 layered clay minerals (i.e., smectite; Chen et al., 2021; Rasmussen et al., 2018; von Fromm et al., 2021; von Fromm et al., 2023; Yu et al., 2021). This is due to their large specific surface areas with a high proportion of reactive sites (Parfitt & Childs, 1988). Furthermore, the occlusion of SOC in stable microaggregates may also contribute to SOC persistence by physically preventing microorganisms from accessing otherwise readily available C sources (Six et al., 2000; Tisdall & Oades, 1982).

With soil depth, SOC abundance usually decreases (Jobbágy & Jackson, 2000; Oades, 1988), whereas SOC persistence (lower $\Delta^{14}C$ values and older SOC ages) increases (Balesdent et al., 2018; He et al., 2016; Shi et al., 2020). This strong depth trend has been the focus of many studies (e.g., Ahrens et al., 2020; Don et al., 2013; Jobbágy & Jackson, 2000; Kaiser & Kalbitz, 2012). Explanations differ among these studies, with the depth-trend attributed to (i) reduced decomposition rates with depth, (ii) changes in above- and belowground C inputs with depth, (iii) time required for vertical C transport by water and (iv) increase in SOC protection (e.g., via mineral adsorption or physical protection) with depth. To better understand which of these factors and processes may dominate SOC dynamics under specific environmental conditions, it is necessary to assess and model their combined effects on SOC abundance and persistence together. Thus, qualitative modeling experiments (i.e., conceptualizing changes in SOC abundance and persistence as a linear system of ordinary differential equations) can be a powerful tool to isolate the role that individual processes play in the relationship between SOC abundance and persistence with soil depth.

All of these processes, and thus SOC abundance and persistence, are influenced and shaped by a combination of climatic, geochemical, and biological factors, which can form distinct pedo-climatic conditions at the global scale. Although SOC abundance and persistence are influenced by similar factors, they may represent aspects of SOC dynamics that are driven by different soil processes. These differences can also influence the relationship between SOC abundance and persistence within a soil profile and thus, result in distinct soil profiles depending on pedo-climatic conditions.

Here, we systematically test differences in controls on SOC abundance and persistence across pedo-climatic regions and with soil depth by using a combination of statistical and depth-resolved compartment models. In this work, we are addressing the following research questions (RQ):

RQ1: How do SOC abundance and persistence covary across pedo-climatic regions and with soil depth?

RQ2: What climatic and mineralogical controls best explain regional differences in SOC abundance and persistence?

RQ3: Which processes control depth profiles of SOC abundance and persistence at the global scale?

2 | METHODS

2.1 | Soil profile selection and radiocarbon analysis

We used a subset of the soil layer data from the International Soil Radiocarbon Database (ISRaD v2.4.7.; Beem-Miller et al., 2021; Lawrence et al., 2020) that included both radiocarbon ($\Delta^{14}C$; ‰; here used as a proxy for the timescales of SOC persistence) and soil organic carbon measurements (SOC; wt-%; here used as a measure for SOC abundance; von Fromm et al., 2024). We report ^{14}C data as $\Delta^{14}C$, which is corrected for the decay of the oxalic acid standard between 1950 and the measurement year. To account for mass-dependent fractionation effects, the reported $^{14}C/^{12}C$ ratio of all samples has been corrected to a common $\delta^{13}C$ value of −25‰ (Stuiver & Polach, 1977).

For our analysis, we focus on bulk soil $\Delta^{14}C$ measurements, which represent a mixture of older and younger SOC, and thus reflect the mean of an often highly skewed distribution of $\Delta^{14}C$ in the sample (Chanca et al., 2022; Sierra et al., 2018). Due to a large increase in atmospheric $\Delta^{14}C$ concentration during intensive nuclear weapons testing in the 1960s ("bomb" C), $\Delta^{14}C$ values >0‰ indicate that most of the SOC cycles on decadal timescales (i.e., less persistent). Values of $\Delta^{14}C < 0$‰ indicate that sufficient time elapsed for radioactive decay and most of the SOC cycles on centennial timescales or even longer (i.e., more persistent; Trumbore, 2009; Sierra et al., 2018). Since $\Delta^{14}C$ measurements are time dependent, we examined the data by year of measurement. We found that two-thirds of the data were collected after 1995. Thus, we did not attempt to correct for potential temporal changes and assumed the decline in atmospheric $\Delta^{14}C$ during the study period has only a small effect on the results, given the relatively longer timescales associated with SOC persistence.

For our analyses, we only included mineral soil profiles (no wetlands/peatlands/Histosols) with $\Delta^{14}C$ and SOC values reported for at least three depth layers. This resulted in a total of 597 profiles from 110 globally distributed studies (Figure 1). The data cover a wide range of climate and soil types (Table S1). However, drier and colder conditions tend to be underrepresented in each climate zone (Figure S1), which is reflected in the spatial bias toward North America ($n_{Profiles} = 257$) and Central Europe ($n_{Profiles} = 85$; Figure 1). More than half of the profiles are from forests (56%), followed by grasslands (19%), croplands (12%), shrublands (6%) and other vegetation types (7%).

2.2 | Identification and grouping of global pedo-climatic regions

Pedo-climatic regions are areas of relatively homogenous soil and climate conditions (Metzger et al., 2005). Particularly at larger scales, they have been proven useful to better understand differences in the controls on SOC dynamics and to account for continental-scale differences in soil age that can cause correlations between mineralogy and climate (von Fromm et al., 2023). For example, temperate and boreal forests in the northern hemisphere are often younger soils with different mineralogical compositions than tropical soils. We combined the reported $\Delta^{14}C$ and SOC data from ISRaD with global climate and soil data, either by using the reported variables or gap-filling based on globally gridded data products by extracting the corresponding values based on longitude and latitude at the profile level. The global data include present-day Köppen–Geiger climate zones (Beck et al., 2018), mean annual precipitation (MAP; mm) and mean annual temperature (MAT;°C; WorldClim v2; Fick & Hijmans, 2017), potential evapotranspiration (PET; mm; Zomer et al., 2022), clay content (%; SoilGrids v1; Hengl et al., 2017), and soil order (USDA; Shi et al., 2020). We had to limit our analyses to these broad climate and soil variables, since more precise data, especially for soil mineralogy, are not available at the global scale. For more information about the exact gap-filling procedure, we refer to the R code (see *Data availability*) and Table S2 which shows the relative number of values gap-filled for each variable. Mean annual precipitation and PET were used to calculate the aridity index, which we defined as PET/MAP (Budyko, 1974). Aridity values >1 indicate water-limited (dry) conditions and ratios <1 represent energy-limited (wet) conditions.

We grouped all soil profiles according to their main climate group and dominant mineral type, respectively. Climate zones were grouped into broad climate groups to ensure that each group contained a sufficient number of soil profiles (Figure S1 and Table S1). The grouping was based on the first capital letter of the Köppen–Geiger classification system, which refers to the five main climate groups, namely A—tropical, B—arid, C—warm temperate, D—cold temperate/continental, and E—polar/tundra (Figure 1; Beck et al., 2018). Profiles that were classified as Gelisols or as Aridisols in the field were manually assigned to the polar/tundra or arid climate group, respectively. Andisols (volcanic/amorphous soils) were excluded from the climate grouping, since they are a geochemically, mineralogically, and pedogenically distinct soil type that are not representative for a given climate zone (Parfitt & Clayden, 1991). We recognize that other azonal soil types (e.g., Entisols, Mollisols, Inceptisols) exist and that climate zones do not capture all soil variability. On a global scale, however, climate groups integrate many soil-forming factors and can be seen as a conservative grouping of soil profiles that may be highly diverse locally but face a similar set of underlying large-scale environmental factors.

Soil types were used to identify dominant mineral groups relevant for SOC abundance and persistence (Figure 1 and Table S1). We used the dominant clay-sized minerals identified by Ito and Wagai (2017) for each soil order as a grouping proxy. All Andisols were classified as dominated by amorphous minerals. These amorphous minerals include mostly allophanes, which are thought to be highly efficient at adsorbing SOC (Torn et al., 1997). Highly dynamic, young, and eroding land surfaces and those experiencing less chemical weathering, such as cold or hot arid regions, or mountainous environments, were grouped as soils dominated by less weathered clays such as illite, or primary minerals such as mica. These soils, including Alfisols, Aridisols, Entisols, Gelisols, and Inceptisols (Ito & Wagai, 2017), have an underdeveloped potential for mineral SOC stabilization (Mathieu et al., 2015) and are generally situated in climate zones less favorable to biological activity. Soils from intermediately aged, often quaternary land surfaces in seasonal or temperate climate zones, were classified as dominated by high-activity clays. They include Mollisols, Spodosols and Vertisols (Ito & Wagai, 2017). These are dominated by smectite and vermiculite, which are characterized by high surface areas and variable charges that can adsorb large amounts of SOC (Khomo et al., 2017; Wattel-Koekkoek et al., 2003). Soils such as Oxisols and Ultisols from stable, often tropical, old land surfaces, were grouped as dominated by low-activity clays, such as kaolinite (Ito & Wagai, 2017). These have a limited surface area and therefore tend to adsorb less SOC (Feller, 1993). We acknowledge that the grouping of dominant mineral groups based on soil orders is an oversimplification of the much more complex soil mineralogy. Yet, this classification is widely used and supported by

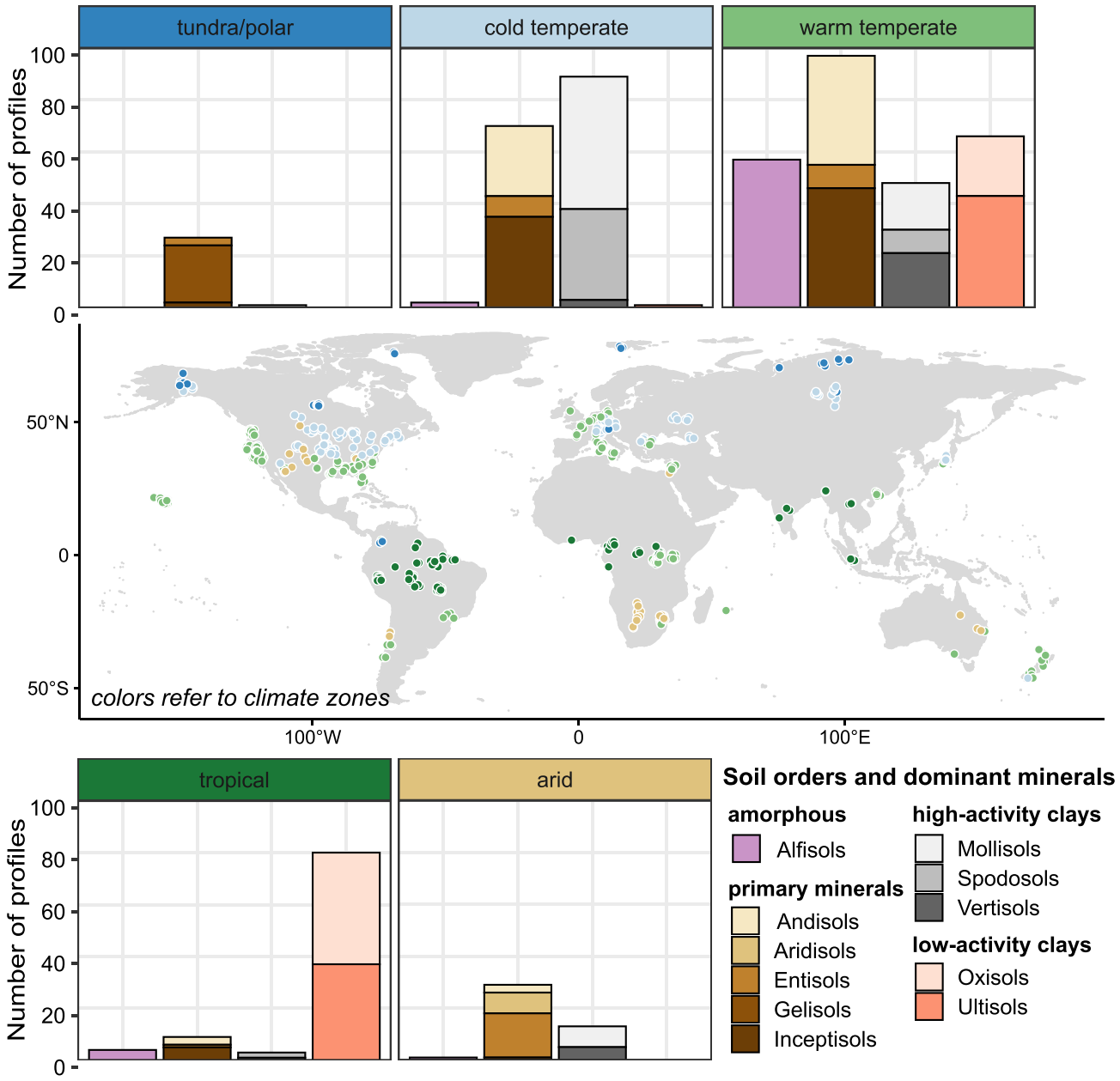

FIGURE 1 Distribution and number of soil profiles across the main climate zones, soil orders and dominant mineral type. Climate zones are based on Köppen–Geiger climate classifications (Beck et al., 2018). Soils are grouped by soil order, with each soil order associated with a dominant mineral type: amorphous = Andisols; primary minerals = Alfisols, Aridisols, Entisols, Gelisols and Inceptisols; high-activity clays = Mollisols, Spodosols, Vertisols; low-activity clays = Oxisols, Ultisols.

analytical data (Georgiou et al., 2022; Ito & Wagai, 2017; Quesada et al., 2020; von Fromm et al., 2023). At present, the only approach that can be used at the global scale where more precise data on soil mineralogy and especially data coexisting with radiocarbon measurements are sparse. This approach also allows us to test the applicability of climate zones and soil orders as a pedo-climatic grouping of soil profiles with respect to SOC abundance and persistence at the global scale.

Overall, the applied climate and mineral grouping results in significantly different groups based on MAP, MAT, and PET, and clay content, respectively (based on Kruskal–Wallis test, followed by a post hoc Dunn test with a Bonferroni correction for the *p*-values; *p*-value <.0001). Only MAP between polar/tundra and arid regions is not significantly different (*p*-value >.5; Figure 2).

2.3 | Sampling depth harmonization

Since the depth intervals at which samples were collected varied across soil profiles in the ISRaD database, it was necessary to harmonize the depth distribution of the data. For this, a mass-preserving spline function (equal-area quadratic smoothing spline) was applied to each profile (Bishop et al., 1999; Ponce-Hernandez

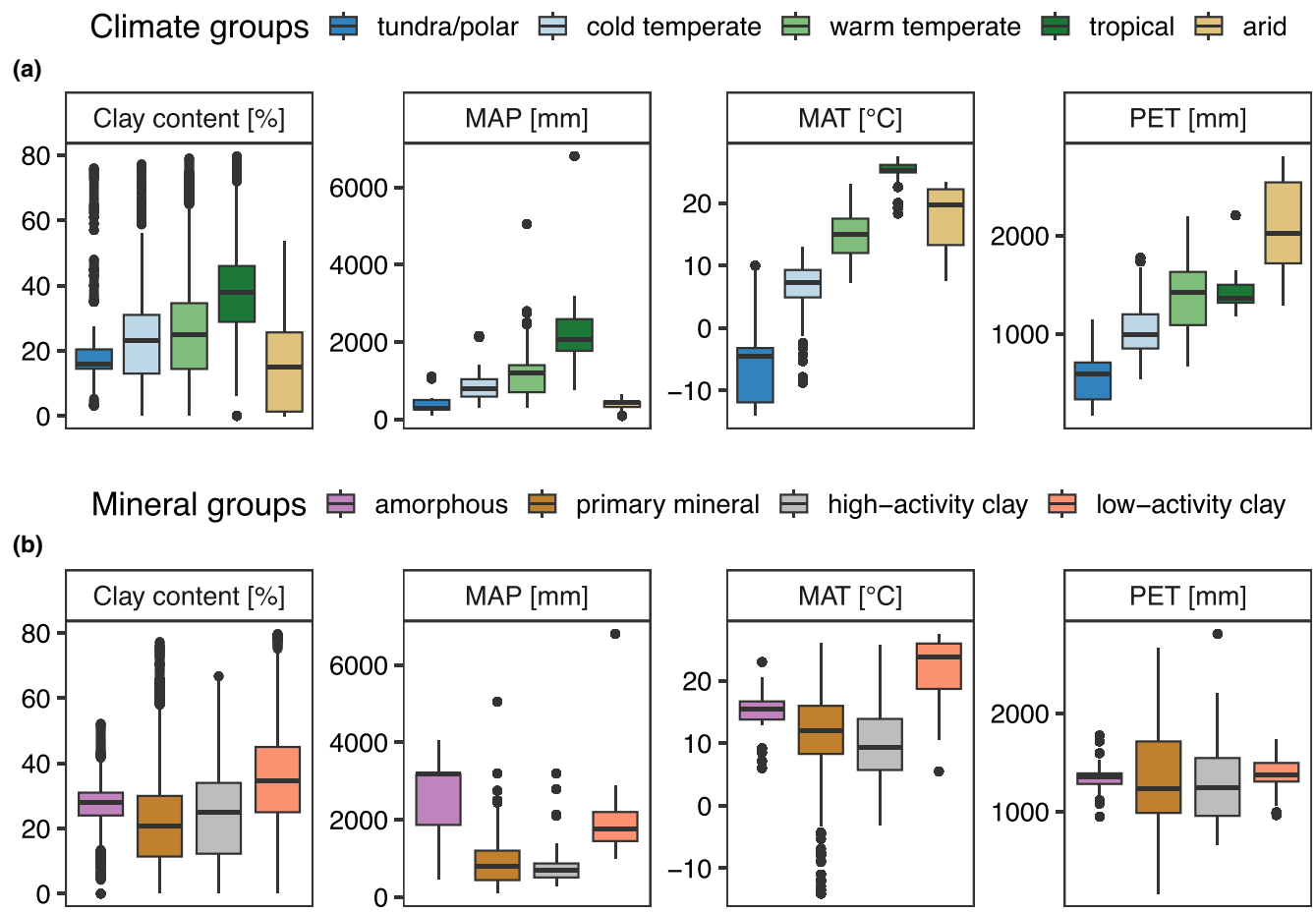

FIGURE 2 Boxplots for clay content, mean annual precipitation (MAP), mean annual temperature (MAT) and mean annual potential evapotranspiration (PET) for (a) climate groups and (b) dominant mineral groups (assigned using soil order classification; see Methods).

et al., 1986). In short, a spline function is a set of local quadratic functions tied together with "knots" that describe a smooth curve through a set of points (in our case sampling depth; Bishop et al., 1999; Malone et al., 2009). The spline function allows for some "smoothing" so that the fitted curve does not have to pass exactly through every sampling point. For each individual profile, we applied the spline function to the $\Delta^{14}C$, SOC, and clay content (<2 µm) data to obtain a value for each parameter for each centimeter of depth, extending to the maximum sampling depth. We used the R package "mpspline2" (O'Brien et al., 2022), which allows users to specify the lowest and highest predicted values, as well as a smoothing parameter for the spline function. To constrain the extrapolation within realistic values, we set the lowest and highest values to 0.005 and 60 wt-%, for $\Delta^{14}C$ to −1000 and + 350‰, and for clay content to 0 and 100%. The smoothing factor was set to 0.5 for each profile. After applying the spline function, we used 100 cm as a cutoff for the maximum sampling depth. This ensured that there were enough data from profiles with deeper sampling depths. However, not all soil profiles in this study reach 100 cm soil depth, and the number of available profiles decreases with increasing soil depth to $n_{Profile} = 290$ at 100 cm. Lastly, since our aim is to understand and represent SOC dynamics in mineral soil layers, we removed all layers with SOC content >20 wt-% after applying the spline function to avoid including organic layers in our analysis.

2.4 | Statistical analyses

We focus on presenting the harmonized soil profile data in a 2D-space consisting of $\Delta^{14}C$ as a measure of SOC persistence, and SOC content as a measure of SOC abundance. In this 2D space, all values are sorted by depth to preserve their occurrence within a soil profile.

2.4.1 | Soil profile comparison

To compare soil profiles across climate and mineral groups, we calculated the median for $\Delta^{14}C$ and SOC within each group for each centimeter, respectively. The Wilcoxon rank-sum test was used to calculate the 95% confidence intervals for each group. At each centimeter soil depth, we ensured that the number of profiles was at least one-third of the total number of profiles in that group, and that these profiles came from at least three different studies and

five different profiles. Due to this filtering, the median profiles for amorphous and polar/tundra soils cover a maximum soil depth of 80 and 90 cm, respectively, and not 100 cm as for the rest of the dataset.

2.4.2 | Statistical modeling

Random forest regressions (Breiman, 2001; Breiman et al., 1984) were used to identify the most important predictors for SOC abundance and persistence in order to better understand the observed patterns between the two target variables. We built one model each for $\Delta^{14}C$ and SOC content with the same explanatory variables: depth, MAT, PET/MAP, and clay content. Note that we did not use the random forest models to do any up-scaling, but to better understand the nonlinear behavior between the target variables ($\Delta^{14}C$ or SOC) and the explanatory variables, and how their importance may differ across pedo-climatic groups. Furthermore, we limited the analysis to these four environmental proxy variables since they (i) have been identified by other studies as being important in explaining variations in $\Delta^{14}C$ and SOC at the global scale (Heckman et al., 2022; Luo et al., 2021; Mathieu et al., 2015; Shi et al., 2020), (ii) integrate a wide range of environmental processes (Wiesmeier et al., 2019), and (iii) contain independent information that allows for a better interpretation of these individual predictors, as they correlate with each other only to a lesser degree at broader scales (Table S3). Furthermore, these variables are widely available at reasonable precision and resolution at the global scale and therefore used by various global models to explain soil responses to climate change (Abramoff et al., 2018; Sulman et al., 2014; Wieder et al., 2014).

Note that only soils from arid, warm temperate, cold temperate, and tropical climate zones were included in the random forest analysis. Andisols and soils from tundra/polar regions had to be excluded because their distinct soil characteristics would strongly influence the model behavior due to the nature of the regression approach. For example, Andisols cover less than 1% of the ice-free land surface area but are over-represented in ISRaD (~10% of all soil profiles included in this study). Only 28 profiles were available in the dataset for tundra/polar profiles from very few clustered sampling regions (Figure 1). Including them in the regression analysis would introduce a strong local bias in the predictive model that is unlikely to be representative of the entire climate zone.

For the validation of the resulting regression models, we performed a 10-fold cross-validation, ensuring that each soil profile was either fully within the training (70%) or the test dataset (30%). Model evaluation was performed on the testing dataset, including the calculation of the (root) mean square error. To assess the importance of each independent variable for the predictive power of the model, we calculated the "permutation feature importance." This measure can be interpreted as an explanatory variable being "important" if the shuffling of its values increases the model error, indicating that the model was relying on that explanatory variable for prediction (Molnar, 2022). To further interpret the outcome of the random forest models, we used partial dependence plots and individual conditional expectation plots. The partial dependence plots show the marginal effects of an explanatory variable on the predicted outcome of the random forest model (Friedman, 2001). The individual conditional expectation plots are similar to partial dependence plots, but instead show a line per observation that shows how an observation's prediction changes when the value of an explanatory variable changes (Goldstein et al., 2015; Molnar, 2022). Rather than plotting a prediction line for each observation, we calculated the median of subsets of observations based on their climate group (which were not included as predictors in the random forest). This allows us to interpret the importance of each explanatory variable in these groups, respectively.

2.4.3 | Compartment models of soil organic carbon decomposition

We used depth-resolved compartment-based decomposition models (i.e., one- and two-pool) to identify which model parameters have an influence on the relationship between SOC abundance and persistence. In these models, bulk soil organic matter is characterized by distinct compartments (pools) with homogenous decomposition rates that can interact with each other (Manzoni & Porporato, 2009; Sierra et al., 2012). The models allow us to test differences in (i) decomposition rates, (ii) above- and belowground C inputs, and (iii) vertical transport of C. One- and two-pool models are widely used to qualitatively assess SOC dynamics in a simplified way (Manzoni & Porporato, 2009).

For the one-pool model, each soil layer is represented by one compartment that is vertically connected with the next compartment to mimic soil depth (Figure S2). For the two-pool model, each soil layer is represented by two compartments to account for different decomposition rates within the same soil layer (i.e., fast vs. slow pool). Similar to the one-pool model, these two compartments are vertically connected with the next two compartments to mimic soil depth (Figure S2). By using these models, we can isolate individual soil processes to better understand their importance for SOC abundance and persistence and with soil depth without the need to constrain the models with observational data. We qualitatively compare the modeled soil profiles with the measured soil profiles to better understand which factors may control differences between their shapes with depth across different pedo-climatic zones.

2.4.3.1 | *Model setup*

We ran the models within the "SoilR" framework (Sierra et al., 2012, 2014) and extended the models by adding a depth-resolved version (vertical transfer linear model). For each model, we defined 10 vertical layers. Each layer represents 10 cm, so that the whole profile represents a soil depth of 1 m. The general model of soil organic matter decomposition is a linear dynamical system of the following form:

$$d\mathbf{C}(t)/dt = \boldsymbol{I} + \mathbf{A}\mathbf{C}(t), \quad (1)$$

where the amount of SOC in different pools is represented as vector $\boldsymbol{C}(t)$, with total SOC inputs (above- and belowground) represented by the vector $\boldsymbol{I}$. The decomposition operator $\boldsymbol{A}$ is a square matrix of dimension $m \times m$, which contains the decomposition rates k_i for each pool i, and, in the case of the two-pool model, the coefficients α_{ij} representing the proportion of SOC transferred between pools within a soil layer (Sierra et al., 2012). For the depth-resolved version, the dimension of the system is increased by the total number of depth layers l. Therefore, the matrix $\boldsymbol{A}$ is extended to dimension $(m \times l) \times (m \times l)$, with off-diagonal coefficients representing both the proportion of SOC transferred vertically from one layer to the next and between pools (Figure S2). Analogously, in the depth-resolved version of the model, the vector of SOC stocks and the vector of SOC inputs are extended to dimension m x l, representing SOC stocks and inputs for each pool at each layer, respectively.

Similarly, the dynamical system for radiocarbon in soil organic matter can be represented as:

$$\mathrm{d}^{14}\mathbf{C}(t)/\mathrm{d}t = \boldsymbol{I}_{14C}(t) + \mathbf{A}^{14}\mathbf{C}(t) - \lambda^{14}\mathbf{C}(t), \quad (2)$$

where the amount of radiocarbon in each pool and depth layer is represented by the vector $^{14}\boldsymbol{C}(t)$, with the radiocarbon inputs represented by $\boldsymbol{I}_{14C}(t)$, and λ as the radioactive decay constant.

Within the framework of "SoilR", SOC stocks and Δ^{14}C values are calculated simultaneously, which allows us to plot the model results in the same 2D space as the harmonized soil profile data. Before estimating Δ^{14}C values and SOC stocks, we ran the model to steady state (50,069 years spin-up with historical atmospheric radiocarbon data until 2019; Hua et al., 2022; Reimer et al., 2013). Steady state was achieved when total C inputs were equal to C outputs (Sierra et al., 2014).

2.4.3.2 | *Application*

We used the one-pool model to investigate the influence of each model parameter on the relationship between SOC stocks and Δ^{14}C within the 2D space of SOC abundance and persistence. The tested parameters included:

(i) Decomposition rates (k) that are constant with soil depth,
(ii) Decomposition rates (k) that are decreasing with soil depth,
(iii) Aboveground C inputs (I_{above}; litter) at the soil surface,
(iv) Belowground C inputs (I_{below}; roots) with soil depth, and
(v) Vertical transfer rates (α) to represent leaching of C down the soil profile.

Note that the range of values applied for each parameter (i–v) is based on expert knowledge and the absolute values of the model outputs are not directly comparable to the raw data. In addition, we recognize that different combinations of model parameter values can lead to similar results (i.e., equifinality). Nevertheless, the qualitative models allow for hypothesis testing and a better understanding of the observed patterns between SOC and Δ^{14}C. For each model scenario, we only changed one parameter (i–v) at a time (Table S4). To have a common model across scenarios (i–v), we defined a reference model with $I_{above} = 1$, which can be interpreted as one unit of SOC entering the soil from aboveground. Therefore, the units of the modeled SOC stocks are arbitrary and easier to interpret. The decomposition rate was set to $k = 1/500$ at each depth layer, which translates to a turnover time of about 500 years. Belowground SOC inputs (I_{below}) were set to 0, except for the model scenario where we tested their influence on SOC stocks and Δ^{14}C. Lastly, the downward transfer rate was set to $\alpha = 0.005$. Since each depth layer has the same length (10 × 10 cm), the transfer rate can be interpreted as the proportional movement of SOC per cm soil in the vertical direction.

The two-pool model was used to test the influence of SOC protection (i.e., by mineral adsorption) on SOC abundance and persistence. Since the only difference between the one- and two-pool models is the movement of C from the "fast" to the "slow" cycling pool, we will focus only on the effect of horizontal C transfer for the two-pool model. This was explored by changing the transfer rate from the "fast" pool (faster decomposition—less C stabilized) to the "slow" pool (slower decomposition—more C stabilized). In theory, the more SOC that enters the "slow" pool, the higher the SOC persistence should be. To test this, we used a model with a k-value of 1/50 for the "fast" pool and of 1/1250 for the "slow" pool. For both pools, the k-values were decreasing with soil depth. We included root inputs (I_{below}) at each depth layer, which were decreasing exponentially. We set $I_{above} = 1$, and the vertical transfer rate to $\alpha = 0.0025$ (Table S4).

All analyses were performed within the R computing environment (version 4.1.1; R Core Team, 2021) including the additional R packages "ggpubr" (Kassambara, 2020), "iml" (Molnar et al., 2018), "mlr3" (Lang et al., 2019), "RColorBrewer" (Neuwirth, 2022), "raster" (Hijmans, 2021), "scales" (Wickham & Seidel, 2022), "sf" (Pebesma, 2018), and "tidyverse" (Wickham et al., 2019).

3 | RESULTS

3.1 | Climate and mineral grouping of SOC abundance and persistence

We found that the 2D space of SOC abundance and persistence provides a useful tool to differentiate between climate and mineral groups at the global scale (Figure 3a,b). The same grouping by climate and mineralogy cannot be resolved when SOC abundance and persistence are mapped in the more typical depth-based approach as indicated by a larger overlap of the 95th confidence intervals (Figure 3c–f).

The climate groups show clear and distinct patterns based on SOC abundance and persistence based on the 95th confidence intervals. Tropical soils show overall the lowest SOC persistence (highest Δ^{14}C values resulting in youngest C) at any given soil depth and the smallest change in SOC persistence (Difference (Δ) in Δ^{14}C = 352‰) between the surface and 1 m soil depth (Figure 3a). Soils from tundra/polar regions have overall a higher SOC abundance and persistence at any given soil depth. This also results in

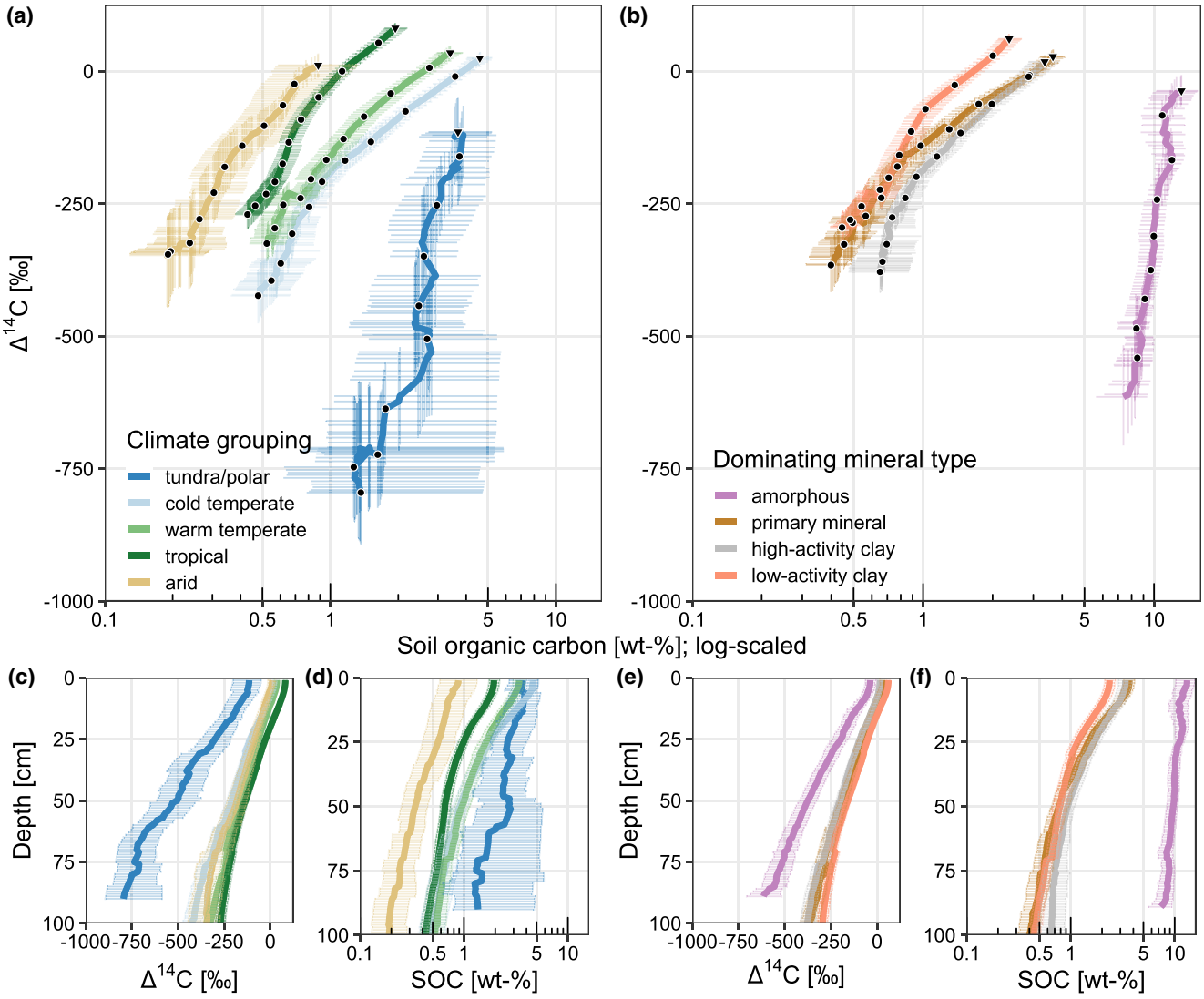

FIGURE 3 Median soil profile data based on harmonized data for $\Delta^{14}C$ and soil organic carbon (SOC) for (a) climate grouping (excluding Andisols) and (b) dominant mineral type. Black dots show 10 cm depth increments and black triangles indicate 0 cm for each group, respectively. (c–f) $\Delta^{14}C$ and SOC plotted against depth for the climate and mineral grouping, respectively. Note that all SOC axes are log-scaled. Error bars show 95% confidence intervals based on the Wilcoxon-Rank-Sum test.

the largest difference of SOC persistence ($\Delta\Delta^{14}C = 739‰$) between the surface and the deepest layer. Temperate soils (warm and cold) show the largest difference in SOC abundance with soil depth (2.88 and 4.14 wt-%, respectively) and the second highest total SOC accumulation after tundra/polar soils. The same is true for the difference in SOC persistence with soil depth compared to the other profiles ($\Delta\Delta^{14}C = 360$ and 449‰, respectively). Arid soils show the smallest accumulation and smallest change of SOC with soil depth (0.70 wt-%) compared to all other groups. In addition, they have relatively high SOC persistence at the surface ($\Delta^{14}C = 11.4‰$), indicating little incorporation of "bomb" ^{14}C (after 1960s), yet the absolute change in SOC persistence with soil depth ($\Delta\Delta^{14}C = 359‰$) is similar to soils from warm temperate and tropical regions.

When grouped by dominant mineralogy, differences between groupings are less pronounced as indicated by the more overlapping 95th confidence intervals. Amorphous soils show the highest accumulation and persistence of SOC (Figure 3b). This is comparable to soils from tundra/polar regions (Figure 3a) and results in a large difference in SOC persistence between the surface and the deepest layer ($\Delta\Delta^{14}C = 677‰$; Figure 3b). Highly weathered soils dominated by low-activity clays show the lowest SOC abundance and persistence at any given soil depth. This also results in the smallest difference in SOC abundance (1.91 wt-%) and persistence ($\Delta\Delta^{14}C = 356‰$) with soil depth. In contrast, moderately weathered soils dominated by high-activity clays have higher SOC abundance and persistence at any given soil depth. The difference in SOC persistence with soil depth ($\Delta\Delta^{14}C = 397‰$) is comparable to soils dominated by primary minerals ($\Delta\Delta^{14}C = 393‰$). Changes in SOC abundance with soil depth are lower for soils dominated by high-activity clays (2.71 wt-%) compared to the primary mineral group (3.26 wt-%). Overall, the differences between the profiles clustered by dominant mineral types are smaller compared to the climate

grouping (except for soils dominated by amorphous minerals) and less clear as suggested by the more overlapping 95th confidence intervals. Therefore, we will focus primarily on climate zones in the remainder of the manuscript.

3.2 | Random forest—Climate and mineral controls

Controls on SOC abundance and persistence differ significantly at the global scale (Figure 4). Both random forest models explain about 55% of the observed variation (SOC abundance: $R^2 = 0.54 \pm 0.15$ and SOC persistence: $R^2 = 0.55 \pm 0.06$) with a root mean square error of 1.5 ± 0.16 w-% and 115 ± 9‰, respectively. For the SOC persistence model ($\Delta^{14}C$), soil depth is the most important predictor (relative importance: 31%), followed by MAT (27%), PET/MAP (23%), and clay content (19%). In contrast, for the SOC abundance model, PET/MAP was the most important predictor (relative importance: 38%), followed by MAT (33%), depth (17%), and clay content (13%; Figure 4). Both models, SOC abundance and persistence, were able to capture differences between climate groups as observed in the harmonized soil profiles, even though the climate groups themselves were not included as predictors in the random forest model (Figure 5; Figure S3). Clay content is the only predictor that covers a wide range within each climate group (Figure 2a), allowing further investigation of its control on SOC abundance and persistence across climate groups (Figure 5).

The effect of clay content on SOC abundance and persistence differs significantly within and between climate groups (Figures 2a and 5). For the SOC persistence model, higher clay content leads to overall more negative predicted $\Delta^{14}C$ values in each climate group—especially in temperate and arid regions (Figure 5a). For the SOC abundance model, higher clay content leads to higher predicted SOC values. Below 30% clay content, all climate groups are significantly different from each other (based on their 95th confidence intervals). In contrast, at higher clay contents, warm and cold temperate soils, and arid and tropical soils are not significantly different from each other, respectively (Figure 5b). When plotting the predicted $\Delta^{14}C$ values against the predicted SOC values for the 95% data range of each climate group (Figure 5c), values with higher clay content (>30%; larger points) fall in the lower right corner (high SOC abundance and persistence), whereas values with lower clay content (<30%; smaller points) fall in the upper left corner (lower SOC abundance and persistence). An exception are tropical soils that show the smallest absolute change in SOC abundance (0.24 wt-%) and persistence (88‰) with clay content (derived by subtracting the predicted SOC/$\Delta^{14}C$ value at the highest clay content from the predicted value at the lowest clay content). This suggests that clay content may not play such an important role in these soils.

3.3 | Depth-resolved compartment models—Parameter testing

We find that a combination of differences in C inputs, decomposition rates and vertical C transport can reasonably explain the observed patterns of SOC abundance and persistence (Figure 6). The identified controls can be linked to our process-understanding gained from the grouping of the soil profiles and from the statistical modeling. The depth-resolved compartment-based decomposition models prove especially useful to separate the influence of (i) decomposition rates, (ii) above- and belowground C inputs, (iii) vertical downward transport, and (iv) SOC protection when visualized within the 2D space of SOC abundance and persistence (Figure 6).

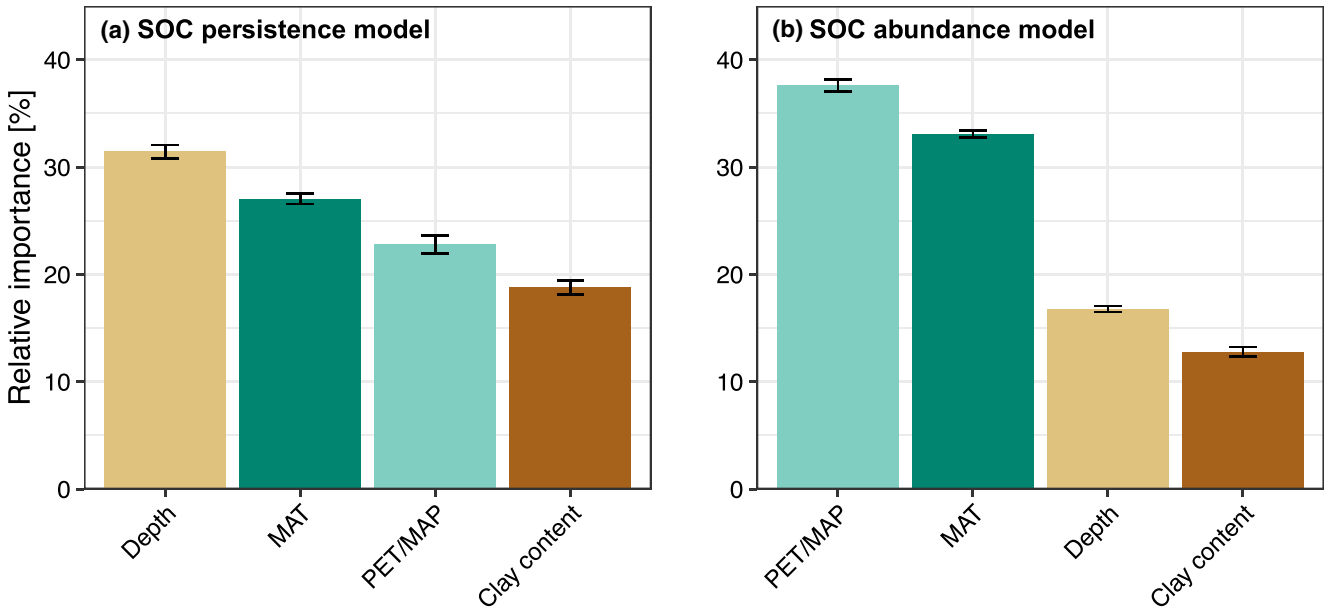

FIGURE 4 Relative variable importance of the random forest models for (a) soil organic carbon (SOC) persistence and (b) SOC abundance. Error bars are calculated from the 10-fold cross-validation and represent the median absolute deviation.

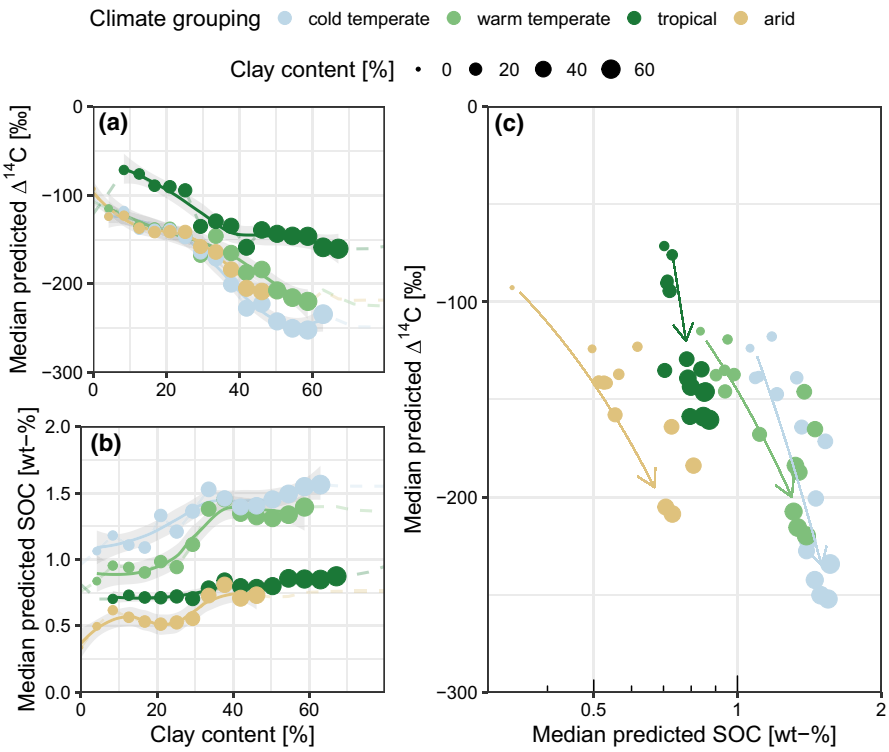

FIGURE 5 Partial dependence plots (PDP) for clay content derived from the random forest model for (a) $\Delta^{14}C$ and (b) soil organic carbon (SOC). In panel (a) and (b), the *y*-axis shows median predicted $\Delta^{14}C$ and SOC values for each observation grouped by their climate group, respectively. Solid lines represent 95% of the respective data range for each climate group (predictions outside this range should be interpreted with caution). Shaded areas refer to the 95th confidence interval. Panel (c) shows median predicted $\Delta^{14}C$ and SOC values for each clay bin (dot size, derived from the PDP) for each climate group, respectively. Arrows indicate change from low to high clay content within each climate group, respectively.

3.3.1 | Decomposition rates

Changes in the decomposition rate lead either to accumulation of SOC with higher SOC persistence (due to slower decomposition) or to lower SOC abundance and persistence (due to faster decomposition; Figure 6b,c). For relatively fast decomposition rates ($k > 1/50$; Figure S4), the highest $\Delta^{14}C$ values are not found at the surface, as usually observed in nature (Figure 3). Due to the rapid decomposition of SOC, more "bomb" ^{14}C (after 1960s) is incorporated deeper into the soil profile, and the models lose more SOC with soil depth (up to 15 orders of magnitude) than is consistent with the harmonized profile data (Figure 3). Varying the decomposition rate with soil depth (Figure 6c) results in soil profile shapes that are more consistent with the harmonized profile data (Figure 3a,b) compared to keeping decomposition rates constant with soil depth.

3.3.2 | Above- and belowground C inputs

In our model experiment, aboveground C inputs (litter) only influence SOC abundance, but not SOC persistence (Figure 6d). This is because these models are at steady state, which means that the C stocks do not change over time and C inputs are balanced by outputs. Therefore, models with overall higher aboveground C inputs have the same SOC persistence as the other models but have higher SOC abundance at each soil depth.

In contrast, belowground C inputs (root inputs) influence both SOC abundance and persistence (Figure 6e). To compare models with different root inputs, we held the sum of root inputs constant (ca. 1.58) and only varied the distribution of C inputs with soil depth. We tested constant, linear, and exponentially decreasing C inputs with depth. Overall, the higher the C inputs with soil depth, the higher the SOC abundance, and the lower the SOC persistence. This is because more fresh (younger) C enters the soil at depth. The distribution of belowground C inputs determines the exact effect of root inputs on SOC abundance and persistence.

3.3.3 | Vertical downward transport

We observed that changes in the vertical downward transport of C can have similar effects on SOC abundance and persistence as changes in root inputs (Figure 6f). With lower rates of vertical transport (smaller α-values), less SOC enters the next soil layer, resulting in overall lower SOC abundance and higher SOC persistence with soil depth. However, the range of tested parameter values can yield

FIGURE 6 Depth-resolved compartment-based decomposition model results. (a) tested model parameters labeled with their corresponding graph, (b) different decomposition rates that are constant with soil depth, (c) changes in decomposition rates with soil depth from no change (vkm.0) to slower decomposition rates (vkm.3), (d) different litter (aboveground C) input quantities, (e) changes in root (belowground C) input distributions; all distributions have a sum of 1.58, (f) different vertical transport rates, (g) different transfer rates from "fast" to "slow" pool and (h) conceptual summary of all models. Black dots in (b–g) represent 10 cm depth increments. Purple thick line in panel (b–f) is always the same reference model. For more details about model parameters see methods and Table S4. Note that *x*-axes are on a log-scale.

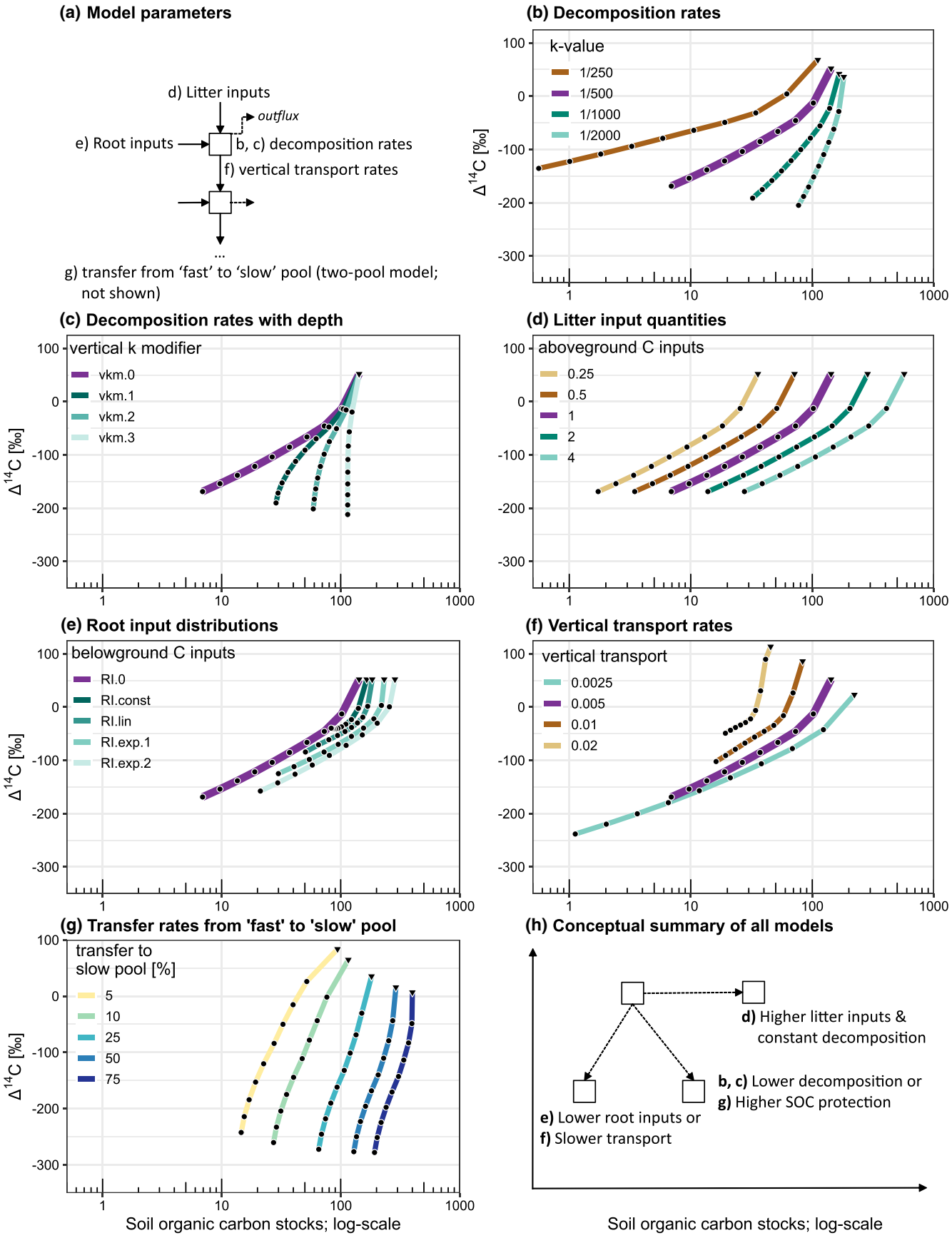

unrealistic results. For example, when the vertical transport rate is small ($\alpha = 0.0001$), the model loses too much SOC with soil depth (up to 12 orders of magnitude; Figure S5) compared to the harmonized profile data (Figure 3). On the other hand, when the vertical downward transport rates are high (for $\alpha > 0.02$), all $\Delta^{14}C$ values are above 0‰, indicating that all depth layers are influenced by "bomb" ^{14}C

(Figure A5), which is again inconsistent with the harmonized profile data (Figure 3).

3.3.4 | Soil organic carbon protection

For the given two-pool model setup, the more SOC that is transferred to the "slow" pool (i.e., higher SOC protection), the higher the SOC abundance and persistence (Figure 6g). Note that the differences in SOC persistence between models decrease with soil depth. This is because less C inputs with high $\Delta^{14}C$ values enter the "fast" pool at depth, and therefore, the influence of the "fast" pool on the "slow" pool decreases with soil depth. In addition, to model similar $\Delta^{14}C$ values with soil depth (< −175‰) as in the harmonized profile data (Figure 3), two pools are needed to ensure that the model does not lose too much SOC too quickly with depth, while still achieving high SOC persistence (lower $\Delta^{14}C$ values).

4 | DISCUSSION

Our analysis demonstrates that different factors explain the global distribution of SOC abundance and persistence to varying degrees of importance (Figure 4). For example, PET/MAP is most important in predicting SOC abundance at the global scale, whereas depth is most important in explaining variations in SOC persistence. This suggests that while SOC abundance and persistence are related, they reflect different aspects of SOC dynamics (Heckman et al., 2021). This finding has important implications for predicting effects of soil management and climate change on future SOC abundance and persistence.

Our results further highlight differences in the relationship between SOC abundance and persistence across pedo-climatic regions (Figure 3). The identified patterns can be related to differences in C inputs (above- and belowground), decomposition rates, as well as vertical and horizontal transfer of C that are characteristic for the different regions (Figure 6; Sierra et al., 2024). In the following section, we discuss the underlying mechanisms controlling SOC abundance and persistence across regions and their implications for assessing the response of SOC abundance and persistence within their pedo-climatic boundary conditions to changes in soil management and climate.

4.1 | Drivers and interactions of SOC abundance and persistence

4.1.1 | Higher SOC abundance and persistence in cold climates and amorphous soils

At the global scale, the highest SOC abundance and persistence are found in geochemically younger, less weathered soils (Figure 3). This group includes soils that occur in cold temperate and polar/tundra climate zones, as well as soils dominated by amorphous minerals, as has previously been observed in numerous site-scale studies (e.g., Basile-Doelsch et al., 2007; Schuur et al., 2008; Torn et al., 1997). These soils are characterized, on average, by a relatively short soil development (<12,000 years). Furthermore, the harmonized soil profiles of these three pedo-climatic groups (cold temperate, polar/tundra and amorphous soils) have in common that they are characterized by a relatively large spread in SOC persistence with soil depth ($\Delta\Delta^{14}C > 449$‰; Figure 3). This is an indication that the deeper soil layers at 1 m are less connected to surface SOC dynamics. Possible explanations include slower decomposition rates, higher SOC adsorption to minerals, slower vertical C transport and/or less C inputs with soil depth as suggested by our compartment models (Figure 6; Ahrens et al., 2020; Sierra et al., 2024). However, the importance of these different controls on SOC abundance and persistence varies widely for the three pedo-climatic groups.

In amorphous soils, the adsorption of SOC to reactive minerals results in higher SOC protection, reduced vertical transport and decomposition rates (Figure 6b,c,f,g; Oades, 1988; Torn et al., 1997). Overall, this makes the SOC in these soils highly persistent against decomposition and climate change (McGrath et al., 2022). In contrast, in polar/tundra soils, low temperatures and high soil moisture typically result in slower decomposition rates and contribute to the accumulation of large SOC stocks over long time periods (Figure 6b,c; Ping et al., 2015; Hugelius et al., 2014; Shi et al., 2020). However, under climate change, these large SOC stocks could be easily decomposed if SOC is not adsorbed by minerals (Gentsch et al., 2018; Hicks Pries et al., 2013; Schuur et al., 2008). Soil organic carbon abundance and persistence in soils from cold temperate regions are most likely controlled by a combination of climate and mineral controls (Rasmussen et al., 2006). These soils still show relatively large differences in SOC persistence between the surface and deeper layers ($\Delta\Delta^{14}C = 449$‰) and intermediate SOC abundance (Figure 3a). This suggests that mineral adsorption of SOC and reduced decomposition rates are more important than vertical transport of SOC and root inputs at deeper depths, resulting in overall more persistent SOC (Figure 6b,c,e,f). Soils from cold temperate regions are also dominated by high-activity clays (Figure 1), which have a greater capacity to adsorb SOC (Rasmussen et al., 2018; Yu et al., 2021), reducing overall decomposition rates and vertical transport of SOC.

4.1.2 | Soils with lower SOC abundance and persistence

Lower SOC abundance and persistence are found in warm temperate, tropical, and arid regions (Figure 3; Mathieu et al., 2015; Shi et al., 2020). These soils are, on average, characterized by a longer soil development (>12,000 years) and are characterized by smaller differences in SOC persistence between the surface and deeper

layers ($\Delta\Delta^{14}C < 360‰$; Figure 3). This suggests that SOC dynamics throughout the soil profile are more closely related, either via faster vertical transport (Kalbitz & Kaiser, 2008) or higher root inputs with soil depth (Jackson et al., 1996) combined with faster decomposition rates as suggested by our compartment models (Figure 6b,c,e,f). However, the importance of these controls on SOC abundance and persistence differs among the three pedo-climatic groups.

Soils from warm temperate regions can efficiently adsorb SOC to reactive minerals (Rasmussen et al., 2018; von Fromm et al., 2021; Yu et al., 2021) similar to soils in cold temperate climates (Figure 3). However, soils in warm temperate regions store less persistent SOC at any given soil depth compared to those in cold temperate climates (Figure 3). Our results and previous literature suggest that climate- and mineral-mediated variations in decomposition rates are the main driver of these observed differences (Rasmussen et al., 2006; Townsend et al., 1995; Trumbore et al., 1996). For example, soils from warmer climates are typically characterized by faster turnover rates due to enhanced SOC decomposition (Carvalhais et al., 2014; Trumbore et al., 1996). However, some warm temperate soils are also dominated by low-activity clays (i.e., kaolinite; Figure 1), that typically adsorb less amounts of SOC, which results in overall less persistent SOC (Khomo et al., 2017; Six et al., 2002; von Fromm et al., 2021; Wattel-Koekkoek et al., 2003). This is supported by our statistical models, which show that increased clay content leads to smaller increases in SOC abundance and persistence for warm temperate soils compared to cold temperate soils (Figure 5).

Tropical soils show the smallest change in SOC abundance and persistence with increasing clay content (Figure 5). This is because these soils are primarily dominated by low-activity clays and other end-member weathering mineral products (Figure 1; Feller, 1993). Due to the lower SOC adsorption by minerals and fast decomposition rates due to high moisture availability (Figure 6b,c,g; Sierra et al., 2021; Xiao et al., 2022), tropical soils have the youngest and least persistent C at any given soil depth (Figure 3). This is also supported by the fact the tropical soils have the deepest incorporation of "bomb" ^{14}C (down to 20 cm; Figure 3) suggesting that these soils exchange C relatively fast (decadal timescales) with the atmosphere.

Arid soils are characterized by relatively high SOC persistence at the surface ($\Delta^{14}C = 11‰$), while deeper soil layers more closely resemble warm temperate and tropical soils (Figure 3). This suggests that only small amounts of fresh C (which would have higher $\Delta^{14}C$ values) enter the soil and that, on average, surface SOC cycles on longer timescales compared to the other two pedo-climatic regions. However, given that arid soils are characterized by the lowest SOC abundance (Figure 3), low C inputs due to low (root) biomass (Jackson et al., 1996) are likely to be the limiting factor rather than reduced decomposition rates due to low moisture availability (Ewing et al., 2008). This is also supported by our compartment models (Figure 6). Mineral SOC adsorption may only play a role in arid soils where high-activity clays are present (Figure 1; Khomo et al., 2017; Quéro et al., 2022), and where higher clay content then leads to higher SOC abundance and persistence (Figure 5).

4.2 | Implications for soil C management

Conceptually, by linking the identified patterns and controls of SOC abundance and persistence to the results of the compartment-based model experiment, our findings can be used to assess region-specific responses of soils to changes in management and climate. Our compartment-based models show that high SOC abundance and persistence required for long-term SOC storage can be found when high C inputs (above- and belowground) are getting adsorbed by minerals and/or are only slowly decomposed (Figure 6h). Based on our findings, we will briefly conceptualize how soil responses will differ across our pedo-climatic regions, using increased C inputs as an example.

Centered on current conditions, soils dominated by high-activity clays from warm and cold temperate regions, followed by soils from arid regions with high-activity clays and high C inputs are characterized by relatively high SOC abundance and persistence due to a combination of high C inputs, mineral C adsorption, and reduced decomposition rates (Figures 3, 5 and 6). In particular, soils from cold temperate regions already store large amounts of SOC under current conditions (ca. 1581 Pg C in the first meter, Hengl et al., 2017). Under increased C inputs, the key challenge will be to ensure that newly added C is decomposed slowly, for example, due to mineral C adsorption. However, many studies have shown that most of the newly entered C, also at deeper depth, is decomposed relatively quickly and is typically not contributing to long-term C storage (Balesdent et al., 2018; Scheibe et al., 2023; Stoner et al., 2021; Xiao et al., 2022).

Our findings imply that tropical soils are the most challenging for increasing long-term SOC storage, since they have relatively low SOC abundance and persistence under current conditions (Figures 3 and 5). Although tropical evergreen forests have the highest root biomass globally (Jackson et al., 1996), most of the C decomposes relatively quickly due to environmental and mineralogical conditions, as indicated by the deepest incorporation of "bomb" C (Figures 3 and 6; Muñoz et al., 2023). In addition, because these soils are highly weathered (i.e., dominated by 1:1 clay minerals; Figure 1), the reactivity of these minerals, and therefore the adsorption of C by minerals, cannot be increased. Therefore, the focus for tropical soils should be on maintaining SOC rather than trying to increase it over longer time periods (Reichenbach et al., 2023). This is particularly important because tropical soils exchange C with the atmosphere on decadal timescales down to 20 cm (Figure 3), suggesting that these soils may respond more rapidly to environmental changes (Nottingham et al., 2020). In addition, due to the large area that tropical soils cover, their absolute SOC storage in the first meter (ca. 515 Pg C) is greater than that of warm temperate soils (ca. 389 Pg C) and arid soils (ca. 318 Pg C; Hengl et al., 2017).

Amorphous soils and soils from polar/tundra regions have the highest SOC abundance and persistence under current climatic conditions (Figure 3). Due to their large amounts of reactive minerals, amorphous soils are likely to be able to store large amounts of SOC

over longer time periods, yet these soils cover <1% of the ice-free land surface area. Soils from polar/tundra regions currently store about 1048 Pg C in the first meter (Hengl et al., 2017), but they are at high risk of releasing large amounts of formerly persistent C due to climate warming (Schuur et al., 2008).

4.3 | Implications for global C modeling

Our findings can be a valuable tool for testing the performance of global C models and their ability to capture key processes relevant to SOC abundance and persistence across regions. Radiocarbon has been established as a powerful tool to constrain C cycling rates in models (Ahrens et al., 2020; Chen et al., 2019; Koven et al., 2013) and for model intercomparison (He et al., 2016; Shi et al., 2020). However, a key challenge is that radiocarbon measurements are only available from a few sites (Lawrence et al., 2020). Therefore, many C models suffer from the difficulty of using information collected at the site level and extrapolating to the global scale (Manzoni & Porporato, 2009; Reichstein & Beer, 2008). Our harmonized soil profiles of SOC abundance and persistence for different pedo-climatic regions provide a promising opportunity to constrain global C models rather than constraining them with individual soil profile data that may not always be generalizable. However, the unique controls on SOC abundance and persistence identified in the pedo-climatic regions limit the ability to extrapolate across these regions—this has also implications for statistical modeling of SOC abundance and persistence.

Future work should focus on the relationship between SOC abundance and persistence over time and in other soil fractions. Using bulk $\Delta^{14}C$ measurements to constrain global C models overlooks the fact that these data represent the mean of mostly highly skewed C age distributions and thus overestimate the C age (Sierra et al., 2018). In addition, some of this very old C may be rock derived. Soils developed from sedimentary rocks may have older SOC ages due to the incorporation of the much older organic C of the parent rock material into the soil matrix (Bukombe et al., 2021; Grant et al., 2023; Kalks et al., 2021; van der Voort et al., 2019). Therefore, analyses that take into account the source of C by using fractions and stable isotopes such as ^{13}C and ^{15}N can further contribute to a better understanding of the controls and interactions between SOC abundance and persistence across regions (Brunn et al., 2014; Heckman et al., 2022; Kohl et al., 2015). Previous studies have already found distinct relationships between SOC abundance and $\delta^{13}C$ (Acton et al., 2013; Brunn et al., 2014). However, some of these data are even less available at the global scale, making their use for benchmarking global C models even more challenging. Therefore, future work and sampling efforts should also focus on including and measuring more diverse soil data.

Lastly, it is important to note that the introduced 2D framework of SOC abundance and persistence with soil depth is time dependent. Due to changes in atmospheric $^{14}CO_2$ concentrations over time, observed patterns of soil $\Delta^{14}C$ will continue to change with time, and this provides an additional model constraint that could be used to distinguish process models that can produce a single time point with multiple parameter combinations. Thus, the proposed 2D framework of SOC abundance and persistence can still be used to benchmark global C models and to identify strategies to maintain SOC abundance and persistence under global change.

5 | CONCLUSIONS

In summary, the diverse mix of methods presented are complementary and allow for a more holistic interpretation of the processes controlling SOC abundance and persistence across regions. Our analysis shows that a combination of broad climate grouping with mineral information (i.e., soil order and clay content) is useful to better understand SOC abundance and persistence at the global scale. Different controls and processes explain the variation in SOC abundance and persistence across pedo-climatic region. This has implications for assessing effects of management and climate change on soils and C modeling efforts.

RQ1: How do SOC abundance and persistence covary across pedo-climatic regions and with soil depth?

For most soil profiles, as depth increases, SOC abundance declines and SOC persistence increases. However, under extreme climatic and mineral conditions, namely soils from polar/tundra regions and amorphous soils, SOC persistence increases with soil depth, whereas SOC abundance does not necessarily decrease.

RQ2: Which climatic and soil-related controls best explain regional differences in SOC abundance and persistence?

Soil organic carbon abundance and persistence reflect different controls, yet their interaction reveals information about SOC dynamics that are distinct for different pedo-climatic regions and with soil depth. For both measures, climate controls contain more information than mineral controls alone at the global scale. However, differences between and within pedo-climatic zones can be related to mineral controls and are key to assessing global C dynamics.

RQ3: Which processes control depth profiles of SOC abundance and persistence at the global scale?

The identified controls can be linked to soil processes that influence the relationship between SOC abundance and persistence as shown by our qualitative compartment model analyses. The model exercises show that some of the parameters, such as lower decomposition rates and higher C protection potential, or lower root inputs and slower vertical transport, can have similar effects on the distributions of soil profiles within the 2D space of SOC abundance and persistence. However, for most soils, vertical changes in decomposition rates and root input distributions are more important than vertical transport. Compared to the SOC abundance and persistence patterns identified from the grouped profile data, the model results obtained from the vertical transport simulations are implausible.

In conclusion, all these findings have implications for assessing effects of management and climate change on soils and for informing C modeling efforts across regions. Our improved understanding of patterns and drivers of SOC abundance and persistence across regions contributes to a more process-oriented modeling of future soil responses to climate change. Importantly, the variable combination

and strength of controls on SOC abundance and persistence in the proposed pedo-climatic regions limit the ability to extrapolate across these regions and into data-poor regions. Furthermore, global C models should be able to accurately represent the identified differences in the relationship between SOC abundance and persistence between pedo-climatic regions and with soil depth.

AUTHOR CONTRIBUTIONS

Sophie F. von Fromm: Conceptualization; data curation; formal analysis; methodology; visualization; writing – original draft; writing – review and editing. **Alison M. Hoyt:** Conceptualization; supervision; writing – review and editing. **Carlos A. Sierra:** Methodology; software; writing – review and editing. **Katerina Georgiou:** Methodology; writing – review and editing. **Sebastian Doetterl:** Conceptualization; supervision; writing – review and editing. **Susan E. Trumbore:** Conceptualization; supervision; writing – review and editing.

ACKNOWLEDGMENTS

The authors thank everyone who contributed data to the International Soil Radiocarbon Database, which made this study possible. SvF received funding from the International Max Planck Research School for Global Biogeochemical Cycles (IMPRS-gBGC). ST and AH acknowledge support from the European Research Council (Horizon 2020 Research and Innovation Program; grant no. 695101; 14Constraint). The authors thank Caitlin Hicks Pries for her valuable comments on an earlier version of this manuscript. Open Access funding enabled and organized by Projekt DEAL.

CONFLICT OF INTEREST STATEMENT

The authors declare that there are no conflicts of interest.

DATA AVAILABILITY STATEMENT

The data that support the findings of this study are openly available on Zenodo at https://zenodo.org/records/10624813. All R code necessary to reproduce the analysis and figures can be found on Github at https://github.com/SophievF/Global_SOC_Abundance_Persistence and Zenodo at https://zenodo.org/records/11105261. All radiocarbon (Δ14C) and ancillary data can be downloaded from Github at https://github.com/International-Soil-Radiocarbon-Database/ISRaD (Beem-Miller et al. 2021).

ORCID

Sophie F. von Fromm https://orcid.org/0000-0002-1820-1455
Alison M. Hoyt https://orcid.org/0000-0003-0813-5084
Carlos A. Sierra https://orcid.org/0000-0003-0009-4169
Katerina Georgiou https://orcid.org/0000-0002-2819-3292
Sebastian Doetterl https://orcid.org/0000-0002-0986-891X
Susan E. Trumbore https://orcid.org/0000-0003-3885-6202

REFERENCES

Abramoff, R., Xu, X., Hartman, M., O'Brien, S., Feng, W., Davidson, E., Finzi, A., Moorhead, D., Schimel, J., Torn, M., & Mayes, M. A. (2018). The millennial model: In search of measurable pools and transformations for modeling soil carbon in the new century. *Biogeochemistry*, *137*(1), 51–71. https://doi.org/10.1007/s10533-017-0409-7

Acton, P., Fox, J., Campbell, E., Rowe, H., & Wilkinson, M. (2013). Carbon isotopes for estimating soil decomposition and physical mixing in well-drained forest soils. *Journal of Geophysical Research: Biogeosciences*, *118*(4), 1532–1545. https://doi.org/10.1002/2013JG002400

Ahrens, B., Guggenberger, G., Rethemeyer, J., John, S., Marschner, B., Heinze, S., Angst, G., Mueller, C. W., Kögel-Knabner, I., Leuschner, C., Hertel, D., Bachmann, J., Reichstein, M., & Schrumpf, M. (2020). Combination of energy limitation and sorption capacity explains 14c depth gradients. *Soil Biology and Biochemistry*, *148*, 107912. https://doi.org/10.1016/j.soilbio.2020.107912

Baldock, J. A., & Skjemstad, J. O. (2000). Role of the soil matrix and minerals in protecting natural organic materials against biological attack. *Organic Geochemistry*, *31*(7), 697–710. https://doi.org/10.1016/S0146-6380(00)00049-8

Balesdent, J., Basile-Doelsch, I., Chadoeuf, J., Cornu, S., Derrien, D., Fekiacova, Z., & Hatté, C. (2018). Atmosphere–soil carbon transfer as a function of soil depth. *Nature*, *559*(7715), 599–602. https://doi.org/10.1038/s41586-018-0328-3

Basile-Doelsch, I., Amundson, R., Stone, W. E. E., Borschneck, D., Bottero, J. Y., Moustier, S., Masin, F., & Colin, F. (2007). Mineral control of carbon pools in a volcanic soil horizon. *Geoderma*, *137*(3), 477–489. https://doi.org/10.1016/j.geoderma.2006.10.006

Basile-Doelsch, I., Balesdent, J., & Pellerin, S. (2020). Reviews and syntheses: The mechanisms underlying carbon storage in soil. *Biogeosciences*, *17*(21), 5223–5242. https://doi.org/10.5194/bg-17-5223-2020

Beck, H. E., Zimmermann, N. E., McVicar, T. R., Vergopolan, N., Berg, A., & Wood, E. F. (2018). Present and future köppen–geiger climate classification maps at 1-km resolution. *Scientific Data*, *5*(1), 180214. https://doi.org/10.1038/sdata.2018.214

Beem-Miller, J., Monroe, G., Hoyt, A. M., Stoner, S., von Fromm, S. F., Lawrence, C. R., & Sierra, C. A. (2021). Israd. (*version 1.7.8*). https://github.com/International-Soil-Radiocarbon-Database/ISRaD/

Bishop, T. F. A., McBratney, A. B., & Laslett, G. M. (1999). Modelling soil attribute depth functions with equal-area quadratic smoothing splines. *Geoderma*, *91*(1), 27–45. https://doi.org/10.1016/S0016-7061(99)00003-8

Breiman, L. (2001). Random forests. *Machine Learning*, *45*(1), 5–32. https://doi.org/10.1023/A:1010933404324

Breiman, L., Friedman, J., Stone, C. J., & Olshen, R. A. (1984). *Classification and regression trees* (p. 368). Taylor & Francis.

Brunn, M., Spielvogel, S., Sauer, T., & Oelmann, Y. (2014). Temperature and precipitation effects on δ13c depth profiles in som under temperate beech forests. *Geoderma*, *235-236*, 146–153. https://doi.org/10.1016/j.geoderma.2014.07.007

Budyko, M. I. (1974). *Climate and life* (p. 508). Academic Press.

Bukombe, B., Fiener, P., Hoyt, A. M., Kidinda, L. K., & Doetterl, S. (2021). Heterotrophic soil respiration and carbon cycling in geochemically distinct African tropical forest soils. *The Soil*, *7*(2), 639–659. https://doi.org/10.5194/soil-7-639-2021

Carvalhais, N., Forkel, M., Khomik, M., Bellarby, J., Jung, M., Migliavacca, M., Mu, M., Saatchi, S., Santoro, M., Thurner, M., Weber, U., Ahrens, B., Beer, C., Cescatti, A., Randerson, J. T., & Reichstein, M. (2014). Global covariation of carbon turnover times with climate in terrestrial ecosystems. *Nature*, *514*(7521), 213–217. https://doi.org/10.1038/nature13731

Chanca, I., Trumbore, S., Macario, K., & Sierra, C. A. (2022). Probability distributions of radiocarbon in open linear compartmental systems at steady-state. *Journal of Geophysical Research: Biogeosciences*, *127*(3), e2021JG006673. https://doi.org/10.1029/2021JG006673

Chen, J., Zhu, Q., Riley, W. J., He, Y., Randerson, J. T., & Trumbore, S. (2019). Comparison with global soil radiocarbon observations

indicates needed carbon cycle improvements in the e3sm land model. *Journal of Geophysical Research: Biogeosciences*, *124*(5), 1098–1114. https://doi.org/10.1029/2018JG004795

Chen, L., Fang, K., Wei, B., Qin, S., Feng, X., Hu, T., Ji, C., & Yang, Y. (2021). Soil carbon persistence governed by plant input and mineral protection at regional and global scales. *Ecology Letters*, *24*(5), 1018–1028. https://doi.org/10.1111/ele.13723

Doetterl, S., Stevens, A., Six, J., Merckx, R., van Oost, K., Casanova Pinto, M., Casanova-Katny, A., Muñoz, C., Boudin, M., Zagal Venegas, E., & Boeckx, P. (2015). Soil carbon storage controlled by interactions between geochemistry and climate. *Nature Geoscience*, *8*(10), 780–783. https://doi.org/10.1038/ngeo2516

Don, A., Rödenbeck, C., & Gleixner, G. (2013). Unexpected control of soil carbon turnover by soil carbon concentration. *Environmental Chemistry Letters*, *11*(4), 407–413. https://doi.org/10.1007/s10311-013-0433-3

Ewing, S. A., Macalady, J. L., Warren-Rhodes, K., McKay, C. P., & Amundson, R. (2008). Changes in the soil c cycle at the arid-hyperarid transition in the atacama desert. *Journal of Geophysical Research: Biogeosciences*, *113*(G2). https://doi.org/10.1029/2007JG000495

Feller, C. (1993). Organic inputs, soil organic matter and functional soil organic compartments in low-activity clay soils in tropical zones. In K. Mulongoy & R. Merckx (Eds.), *Soil organic matter and dynamics and sustainability of tropical agriculture* (pp. 77–88). John Wiley & Son.

Fick, S. E., & Hijmans, R. J. (2017). Worldclim 2: New 1-km spatial resolution climate surfaces for global land areas. *International Journal of Climatology*, *37*(12), 4302–4315. https://doi.org/10.1002/joc.5086

Friedman, J. H. (2001). Greedy function approximation: A gradient boosting machine. *Annals of Statistics*, *29*(5), 1189–1232. https://doi.org/10.1214/aos/1013203451

Gentsch, N., Wild, B., Mikutta, R., Čapek, P., Diáková, K., Schrumpf, M., Turner, S., Minnich, C., Schaarschmidt, F., Shibistova, O., Schnecker, J., Urich, T., Gittel, A., Šantrůčková, H., Bárta, J., Lashchinskiy, N., Fuß, R., Richter, A., & Guggenberger, G. (2018). Temperature response of permafrost soil carbon is attenuated by mineral protection. *Global Change Biology*, *24*(8), 3401–3415. https://doi.org/10.1111/gcb.14316

Georgiou, K., Jackson, R. B., Vindušková, O., Abramoff, R. Z., Ahlström, A., Feng, W., Harden, J. W., Pellegrini, A. F. A., Polley, H. W., Soong, J. L., Riley, W. J., & Torn, M. S. (2022). Global stocks and capacity of mineral-associated soil organic carbon. *Nature Communications*, *13*(1), 3797. https://doi.org/10.1038/s41467-022-31540-9

Goldstein, A., Kapelner, A., Bleich, J., & Pitkin, E. (2015). Peeking inside the black box: Visualizing statistical learning with plots of individual conditional expectation. *Journal of Computational and Graphical Statistics*, *24*(1), 44–65. https://doi.org/10.1080/10618600.2014.907095

Grant, K. E., Hilton, R. G., & Galy, V. V. (2023). Global patterns of radiocarbon depletion in subsoil linked to rock-derived organic carbon. *Geochemical Perspectives Letters*, *25*, 36–40. https://doi.org/10.7185/geochemlet.2312

He, Y., Trumbore, S. E., Torn, M. S., Harden, J. W., Vaughn, L. J. S., Allison, S. D., & Randerson, J. T. (2016). Radiocarbon constraints imply reduced carbon uptake by soils during the 21st century. *Science*, *353*(6306), 1419–1424. https://doi.org/10.1126/science.aad4273

Heckman, K., Hicks Pries, C. E., Lawrence, C. R., Rasmussen, C., Crow, S. E., Hoyt, A. M., von Fromm, S. F., Shi, Z., Stoner, S., McGrath, C., Beem-Miller, J., Berhe, A. A., Blankinship, J. C., Keiluweit, M., Marín-Spiotta, E., Monroe, J. G., Plante, A. F., Schimel, J., Sierra, C. A., … Wagai, R. (2022). Beyond bulk: Density fractions explain heterogeneity in global soil carbon abundance and persistence. *Global Change Biology*, *28*(3), 1178–1196. https://doi.org/10.1111/gcb.16023

Heckman, K. A., Nave, L. E., Bowman, M., Gallo, A., Hatten, J. A., Matosziuk, L. M., Possinger, A. R., SanClements, M., Strahm, B. D., Weiglein, T. L., Rasmussen, C., & Swanston, C. W. (2021). Divergent controls on carbon concentration and persistence between forests and grasslands of the conterminous us. *Biogeochemistry*, *156*(1), 41–56. https://doi.org/10.1007/s10533-020-00725-z

Heckman, K. A., Possinger, A. R., Badgley, B. D., Bowman, M. M., Gallo, A. C., Hatten, J. A., Nave, L. E., SanClements, M. D., Swanston, C. W., Weiglein, T. L., Wieder, W. R., & Strahm, B. D. (2023). Moisture-driven divergence in mineral-associated soil carbon persistence. *Proceedings of the National Academy of Sciences*, *120*(7), e2210044120. https://doi.org/10.1073/pnas.2210044120

Hengl, T., Mendes de Jesus, J., Heuvelink, G. B. M., Ruiperez Gonzalez, M., Kilibarda, M., Blagotić, A., Shangguan, W., Wright, M. N., Geng, X., Bauer-Marschallinger, B., Guevara, M. A., Vargas, R., MacMillan, R. A., Batjes, N. H., Leenaars, J. G. B., Ribeiro, E., Wheeler, I., Mantel, S., & Kempen, B. (2017). Soilgrids250m: Global gridded soil information based on machine learning. *PLoS One*, *12*(2), e0169748. https://doi.org/10.1371/journal.pone.0169748

Hicks Pries, C. E., Schuur, E. A. G., & Crummer, K. G. (2013). Thawing permafrost increases old soil and autotrophic respiration in tundra: Partitioning ecosystem respiration using δ13c and Δ14c. *Global Change Biology*, *19*(2), 649–661. https://doi.org/10.1111/gcb.12058

Hijmans, R. J. (2021). *Raster: Geographic data analysis and modeling*. https://CRAN.R-project.org/package=raster.

Hua, Q., Turnbull, J. C., Santos, G. M., Rakowski, A. Z., Ancapichún, S., De Pol-Holz, R., Hammer, S., Lehman, S. J., Levin, I., Miller, J. B., Palmer, J. G., & Turney, C. S. M. (2022). Atmospheric radiocarbon for the period of 1950-2019. *Radiocarbon*, *64*(4), 723–745. https://doi.org/10.1017/RDC.2021.95

Hugelius, G., Strauss, J., Zubrzycki, S., Harden, J. W., Schuur, E. A. G., Ping, C. L., Schirrmeister, L., Grosse, G., Michaelson, G. J., Koven, C. D., O'Donnell, J. A., Elberling, B., Mishra, U., Camill, P., Yu, Z., Palmtag, J., & Kuhry, P. (2014). Estimated stocks of circumpolar permafrost carbon with quantified uncertainty ranges and identified data gaps. *Biogeosciences*, *11*(23), 6573–6593. https://doi.org/10.5194/bg-11-6573-2014

Ito, A., & Wagai, R. (2017). Global distribution of clay-size minerals on land surface for biogeochemical and climatological studies. *Scientific Data*, *4*(170103), 1–11. https://doi.org/10.1038/sdata.2017.103

Jackson, R. B., Canadell, J., Ehleringer, J. R., Mooney, H. A., Sala, O. E., & Schulze, E. D. (1996). A global analysis of root distributions for terrestrial biomes. *Oecologia*, *108*(3), 389–411. https://doi.org/10.1007/BF00333714

Jobbágy, E. G., & Jackson, R. B. (2000). The vertical distribution of soil organic carbon and its relation to climate and vegetation. *Ecological Applications*, *10*(2), 423–436. https://doi.org/10.1890/1051-0761(2000)010[0423:Tvdoso]2.0.Co;2

Kaiser, K., & Kalbitz, K. (2012). Cycling downwards—Dissolved organic matter in soils. *Soil Biology and Biochemistry*, *52*, 29–32. https://doi.org/10.1016/j.soilbio.2012.04.002

Kalbitz, K., & Kaiser, K. (2008). Contribution of dissolved organic matter to carbon storage in forest mineral soils. *Journal of Plant Nutrition and Soil Science*, *171*(1), 52–60. https://doi.org/10.1002/jpln.200700043

Kalks, F., Noren, G., Mueller, C. W., Helfrich, M., Rethemeyer, J., & Don, A. (2021). Geogenic organic carbon in terrestrial sediments and its contribution to total soil carbon. *The Soil*, *7*(2), 347–362. https://doi.org/10.5194/soil-7-347-2021

Kassambara, A. (2020). *Ggpubr: 'Ggplot2' based publication ready plots*. https://CRAN.R-project.org/package=ggpubr.

Khomo, L., Trumbore, S., Bern, C. R., & Chadwick, O. A. (2017). Timescales of carbon turnover in soils with mixed crystalline mineralogies. *The Soil*, *3*(1), 17–30. https://doi.org/10.5194/soil-3-17-2017

Kohl, L., Laganière, J., Edwards, K. A., Billings, S. A., Morrill, P. L., Van Biesen, G., & Ziegler, S. E. (2015). Distinct fungal and bacterial δ13c signatures as potential drivers of increasing δ13c of soil organic matter with depth. *Biogeochemistry*, *124*(1), 13–26. https://doi.org/10.1007/s10533-015-0107-2

Koven, C. D., Riley, W. J., Subin, Z. M., Tang, J. Y., Torn, M. S., Collins, W. D., Bonan, G. B., Lawrence, D. M., & Swenson, S. C. (2013). The

effect of vertically resolved soil biogeochemistry and alternate soil c and n models on c dynamics of clm4. *Biogeosciences*, *10*(11), 7109–7131. https://doi.org/10.5194/bg-10-7109-2013

Lang, M., Binder, M., Richter, J., Schratz, P., Pfisterer, F., Coors, S., Au, Q., Casalicchio, G., Kotthoff, L., & Bischl, B. (2019). Mlr3: A modern object-oriented machine learning framework in r. *Journal of Open Source Software*, *4*(44). https://doi.org/10.21105/joss.01903

Lawrence, C. R., Beem-Miller, J., Hoyt, A. M., Monroe, G., Sierra, C. A., Stoner, S., Heckman, K., Blankinship, J. C., Crow, S. E., McNicol, G., Trumbore, S., Levine, P. A., Vindušková, O., Todd-Brown, K., Rasmussen, C., Hicks Pries, C. E., Schädel, C., McFarlane, K., Doetterl, S., … Wagai, R. (2020). An open-source database for the synthesis of soil radiocarbon data: International soil radiocarbon database (israd) version 1.0. *Earth System Science Data*, *12*(1), 61–76. https://doi.org/10.5194/essd-12-61-2020

Luo, Z., Viscarra-Rossel, R. A., & Qian, T. (2021). Similar importance of edaphic and climatic factors for controlling soil organic carbon stocks of the world. *Biogeosciences*, *18*(6), 2063–2073. https://doi.org/10.5194/bg-18-2063-2021

Malone, B. P., McBratney, A. B., Minasny, B., & Laslett, G. M. (2009). Mapping continuous depth functions of soil carbon storage and available water capacity. *Geoderma*, *154*(1), 138–152. https://doi.org/10.1016/j.geoderma.2009.10.007

Manzoni, S., & Porporato, A. (2009). Soil carbon and nitrogen mineralization: Theory and models across scales. *Soil Biology and Biochemistry*, *41*(7), 1355–1379. https://doi.org/10.1016/j.soilbio.2009.02.031

Mathieu, J. A., Hatté, C., Balesdent, J., & Parent, É. (2015). Deep soil carbon dynamics are driven more by soil type than by climate: A worldwide meta-analysis of radiocarbon profiles. *Global Change Biology*, *21*(11), 4278–4292. https://doi.org/10.1111/gcb.13012

McGrath, C. R., Hicks Pries, C. E., Nguyen, N., Glazer, B., Lio, S., & Crow, S. E. (2022). Minerals limit the deep soil respiration response to warming in a tropical andisol. *Biogeochemistry*, *161*(2), 85–99. https://doi.org/10.1007/s10533-022-00965-1

Metzger, M. J., Bunce, R. G. H., Jongman, R. H. G., Mücher, C. A., & Watkins, J. W. (2005). A climatic stratification of the environment of Europe. *Global Ecology and Biogeography*, *14*(6), 549–563. https://doi.org/10.1111/j.1466-822x.2005.00190.x

Molnar, C. (2022). Interpretable machine learning: A guide for making black box models explainable. (2nd ed.).

Molnar, C., Bischl, B., & Casalicchio, G. (2018). Iml: An r package for interpretable machine learning. *Journal of Open Source Software*, *3*(26), 786. https://doi.org/10.21105/joss.00786

Muñoz, E., Chanca, I., & Sierra, C. A. (2023). Increased atmospheric CO_2 and the transit time of carbon in terrestrial ecosystems. *Global Change Biology*, *29*(23), 6441–6452. https://doi.org/10.1111/gcb.16961

Neuwirth, E. (2022). *Rcolorbrewer: Colorbrewer palettes*. https://CRAN.R-project.org/package=RColorBrewer.

Nottingham, A. T., Meir, P., Velasquez, E., & Turner, B. L. (2020). Soil carbon loss by experimental warming in a tropical forest. *Nature*, *584*(7820), 234–237. https://doi.org/10.1038/s41586-020-2566-4

Oades, J. M. (1988). The retention of organic matter in soils. *Biogeochemistry*, *5*(1), 35–70. https://doi.org/10.1007/BF02180317

O'Brien, L., Malone, B. P., Hengl, T., Bishop, T. F. A., Rossiter, D., & Beaudette, D. B. A. (2022). *Mpspline2: Mass-preserving spline functions for soil data*. https://cran.r-project.org/web/packages/mpspline2/index.html.

Parfitt, R., & Childs, C. (1988). Estimation of forms of fe and al—A review, and analysis of contrasting soils by dissolution and mossbauer methods. *Soil Research*, *26*(1), 121–144. https://doi.org/10.1071/SR9880121

Parfitt, R. L., & Clayden, B. (1991). Andisols—The development of a new order in soil taxonomy. *Geoderma*, *49*(3), 181–198. https://doi.org/10.1016/0016-7061(91)90075-5

Pebesma, E. (2018). Simple features for r: Standardized support for spatial vector data. *The R Journal*, *10*(1), 439–446. https://doi.org/10.32614/RJ-2018-009

Ping, C. L., Jastrow, J. D., Jorgenson, M. T., Michaelson, G. J., & Shur, Y. L. (2015). Permafrost soils and carbon cycling. *The Soil*, *1*(1), 147–171. https://doi.org/10.5194/soil-1-147-2015

Ponce-Hernandez, R., Marriot, F. H. C., & Becket, P. H. T. (1986). An improved method for reconstructing a soil profile from analyses of a small number of samples. *Journal of Soil Science*, *37*(3), 455–467. https://doi.org/10.1111/j.1365-2389.1986.tb00377.x

Quéro, S., Hatté, C., Cornu, S., Duvivier, A., Cam, N., Jamoteau, F., Borschneck, D., & Basile-Doelsch, I. (2022). Dynamics of carbon loss from an arenosol by a forest to vineyard land use change on a centennial scale. *The Soil*, *8*(2), 517–539. https://doi.org/10.5194/soil-8-517-2022

Quesada, C. A., Paz, C., Oblitas Mendoza, E., Phillips, O. L., Saiz, G., & Lloyd, J. (2020). Variations in soil chemical and physical properties explain basin-wide amazon forest soil carbon concentrations. *The Soil*, *6*(1), 53–88. https://doi.org/10.5194/soil-6-53-2020

R Core Team. (2021). *R: A language and environment for statistical computing*. Vienna, Austria, https://www.R-project.org/

Rasmussen, C., Heckman, K., Wieder, W. R., Keiluweit, M., Lawrence, C. R., Berhe, A. A., Blankinship, J. C., Crow, S. E., Druhan, J. L., Hicks Pries, C. E., Marin-Spiotta, E., Plante, A. F., Schädel, C., Schimel, J. P., Sierra, C. A., Thompson, A., & Wagai, R. (2018). Beyond clay: Towards an improved set of variables for predicting soil organic matter content. *Biogeochemistry*, *137*(3), 297–306. https://doi.org/10.1007/s10533-018-0424-3

Rasmussen, C., Southard, R. J., & Horwath, W. R. (2006). Mineral control of organic carbon mineralization in a range of temperate conifer forest soils. *Global Change Biology*, *12*(5), 834–847. https://doi.org/10.1111/j.1365-2486.2006.01132.x

Reichenbach, M., Fiener, P., Hoyt, A., Trumbore, S., Six, J., & Doetterl, S. (2023). Soil carbon stocks in stable tropical landforms are dominated by geochemical controls and not by land use. *Global Change Biology*, *29*(9), 2591–2607. https://doi.org/10.1111/gcb.16622

Reichstein, M., & Beer, C. (2008). Soil respiration across scales: The importance of a model–data integration framework for data interpretation. *Journal of Plant Nutrition and Soil Science*, *171*(3), 344–354. https://doi.org/10.1002/jpln.200700075

Reimer, P. J., Bard, E., Bayliss, A., Beck, J. W., Blackwell, P. G., Ramsey, C. B., Buck, C. E., Cheng, H., Edwards, R. L., Friedrich, M., Grootes, P. M., Guilderson, T. P., Haflidason, H., Hajdas, I., Hatté, C., Heaton, T. J., Hoffmann, D. L., Hogg, A. G., Hughen, K. A., … van der Plicht, J. (2013). Intcal13 and marine13 radiocarbon age calibration curves 0–50,000 years cal bp. *Radiocarbon*, *55*(4), 1869–1887. https://doi.org/10.2458/azu_js_rc.55.16947

Scheibe, A., Sierra, C. A., & Spohn, M. (2023). Recently fixed carbon fuels microbial activity several meters below the soil surface. *Biogeosciences*, *20*(4), 827–838. https://doi.org/10.5194/bg-20-827-2023

Schuur, E. A. G., Bockheim, J., Canadell, J. G., Euskirchen, E., Field, C. B., Goryachkin, S. V., Hagemann, S., Kuhry, P., Lafleur, P. M., Lee, H., Mazhitova, G., Nelson, F. E., Rinke, A., Romanovsky, V. E., Shiklomanov, N., Tarnocai, C., Venevsky, S., Vogel, J. G., & Zimov, S. A. (2008). Vulnerability of permafrost carbon to climate change: Implications for the global carbon cycle. *Bioscience*, *58*(8), 701–714. https://doi.org/10.1641/b580807

Shi, Z., Allison, S. D., He, Y., Levine, P. A., Hoyt, A. M., Beem-Miller, J., Zhu, Q., Wieder, W. R., Trumbore, S., & Randerson, J. T. (2020). The age distribution of global soil carbon inferred from radiocarbon measurements. *Nature Geoscience*, *13*(8), 555–559. https://doi.org/10.1038/s41561-020-0596-z

Sierra, C. A., Ahrens, B., Bolinder, M. A., Braakhekke, M. C., von Fromm, S., Kätterer, T., Luo, Z., Parvin, N., & Wang, G. (2024). Carbon sequestration in the subsoil and the time required to stabilize carbon

for climate change mitigation. *Global Change Biology*, *30*(1), e17153. https://doi.org/10.1111/gcb.17153

Sierra, C. A., Estupinan-Suarez, L. M., & Chanca, I. (2021). The fate and transit time of carbon in a tropical forest. *Journal of Ecology*, *109*(8), 2845–2855. https://doi.org/10.1111/1365-2745.13723

Sierra, C. A., Hoyt, A. M., He, Y., & Trumbore, S. E. (2018). Soil organic matter persistence as a stochastic process: Age and transit time distributions of carbon in soils. *Global Biogeochemical Cycles*, *32*(10), 1574–1588. https://doi.org/10.1029/2018GB005950

Sierra, C. A., Müller, M., & Trumbore, S. E. (2012). Models of soil organic matter decomposition: The soilr package, version 1.0. *Geoscientific Model Development*, *5*(4), 1045–1060. https://doi.org/10.5194/gmd-5-1045-2012

Sierra, C. A., Müller, M., & Trumbore, S. E. (2014). Modeling radiocarbon dynamics in soils: Soilr version 1.1. *Geoscientific Model Development*, *7*(5), 1919–1931. https://doi.org/10.5194/gmd-7-1919-2014

Six, J., Conant, R. T., Paul, E. A., & Paustian, K. (2002). Review: Stabilization mechanisms of soil organic matter: Implications for c-saturation of soils. *Plant and Soil*, *241*(2), 155–176. https://doi.org/10.1023/A:1016125726789

Six, J., Elliott, E. T., & Paustian, K. (2000). Soil structure and soil organic matter ii. A normalized stability index and the effect of mineralogy. *Soil Science Society of America Journal*, *64*(3), 1042–1049. https://doi.org/10.2136/sssaj2000.6431042x

Stoner, S. W., Hoyt, A. M., Trumbore, S., Sierra, C. A., Schrumpf, M., Doetterl, S., Baisden, W. T., & Schipper, L. A. (2021). Soil organic matter turnover rates increase to match increased inputs in grazed grasslands. *Biogeochemistry*, *156*(1), 145–160. https://doi.org/10.1007/s10533-021-00838-z

Stuiver, M., & Polach, H. A. (1977). Discussion reporting of 14c data. *Radiocarbon*, *19*(3), 355–363. https://doi.org/10.1017/S0033822200003672

Sulman, B. N., Phillips, R. P., Oishi, A. C., Shevliakova, E., & Pacala, S. W. (2014). Microbe-driven turnover offsets mineral-mediated storage of soil carbon under elevated co2. *Nature Climate Change*, *4*(12), 1099–1102. https://doi.org/10.1038/nclimate2436

Tisdall, J. M., & Oades, J. M. (1982). Organic matter and water-stable aggregates in soils. *Journal of Soil Science*, *33*(2), 141–163. https://doi.org/10.1111/j.1365-2389.1982.tb01755.x

Torn, M., Trumbore, S., Chadwick, O., Vitousek, P., & Hendricks, D. (1997). Mineral control of soil organic carbon storage and turnover. *Nature*, *389*, 170–173. https://doi.org/10.1038/38260

Townsend, A. R., Vitousek, P. M., & Trumbore, S. E. (1995). Soil organic matter dynamics along gradients in temperature and land use on the Island of hawaii. *Ecology*, *76*(3), 721–733. https://doi.org/10.2307/1939339

Trumbore, S. (2009). Radiocarbon and soil carbon dynamics. *Annual Review of Earth and Planetary Sciences*, *37*(1), 47–66. https://doi.org/10.1146/annurev.earth.36.031207.124300

Trumbore, S. E., Chadwick, O. A., & Amundson, R. (1996). Rapid exchange between soil carbon and atmospheric carbon dioxide driven by temperature change. *Science*, *272*(5260), 393–396. https://doi.org/10.1126/science.272.5260.393

van der Voort, T. S., Mannu, U., Hagedorn, F., McIntyre, C., Walthert, L., Schleppi, P., Haghipour, N., & Eglinton, T. I. (2019). Dynamics of deep soil carbon—Insights from 14c time series across a climatic gradient. *Biogeosciences*, *16*(16), 3233–3246. https://doi.org/10.5194/bg-16-3233-2019

von Fromm, S. F., Doetterl, S., Butler, B. M., Aynekulu, E., Berhe, A. A., Haefele, S. M., McGrath Steve, P., Shepherd, K. D., Six, J., Tamene, L., Tondoh, E. J., Vågen, T.-G., Winowiecki, L. A., Trumbore Susan, E., & Hoyt, A. M. (2023). Controls on timescales of soil organic carbon persistence across sub-saharan africa. *Global Change Biology*, *30*, e17089. https://doi.org/10.1111/gcb.17089

von Fromm, S. F., Hoyt, A., Sierra, C. A., Georgiou, K., Doetterl, S., & Trumbore, S. (2024). Supporting material for von Fromm et al (2024) Global synthesis of SOC abundance and persistence profile data [data set]. *Zenodo*. https://doi.org/10.5281/zenodo.10624813

von Fromm, S. F., Hoyt, A. M., Lange, M., Acquah, G. E., Aynekulu, E., Berhe, A. A., Haefele, S. M., McGrath, S. P., Shepherd, K. D., Sila, A. M., Six, J., Towett, E. K., Trumbore, S. E., Vågen, T. G., Weullow, E., Winowiecki, L. A., & Doetterl, S. (2021). Continental-scale controls on soil organic carbon across sub-saharan africa. *The Soil*, *7*(1), 305–332. https://doi.org/10.5194/soil-7-305-2021

Wattel-Koekkoek, E. J. W., Buurman, P., van Der Plicht, J., Wattel, E., & van Breemen, N. (2003). Mean residence time of soil organic matter associated with kaolinite and smectite. *European Journal of Soil Science*, *54*(2), 269–278. https://doi.org/10.1046/j.1365-2389.2003.00512.x

Wickham, H., Averick, M., Bryan, J., Chang, W., D'Agostino McGowan, L., François, R., Grolemund, G., Hayes, A., Henry, L., Hester, J., Kuhn, M., Pedersen, T. L., Miller, E., Bache, S. M., Müller, K., Ooms, J., Robinson, D., Seidel, D. P., Spinu, V., … Yutani, H. (2019). Welcome to the tidyverse. *Journal of Open Source Software*, *4*(43), 1686. https://doi.org/10.21105/joss.01686

Wickham, H., & Seidel, D. P. (2022). *Scales: Scale functions for visualization*. https://CRAN.R-project.org/package=scales.

Wieder, W. R., Grandy, A. S., Kallenbach, C. M., & Bonan, G. B. (2014). Integrating microbial physiology and physio-chemical principles in soils with the microbial-mineral carbon stabilization (mimics) model. *Biogeosciences*, *11*(14), 3899–3917. https://doi.org/10.5194/bg-11-3899-2014

Wieder, W. R., Hartman, M. D., Sulman, B. N., Wang, Y.-P., Koven, C. D., & Bonan, G. B. (2018). Carbon cycle confidence and uncertainty: Exploring variation among soil biogeochemical models. *Global Change Biology*, *24*(4), 1563–1579. https://doi.org/10.1111/gcb.13979

Wiesmeier, M., Urbanski, L., Hobley, E., Lang, B., von Lützow, M., Marin-Spiotta, E., van Wesemael, B., Rabot, E., Ließ, M., Garcia-Franco, N., Wollschläger, U., Vogel, H.-J., & Kögel-Knabner, I. (2019). Soil organic carbon storage as a key function of soils—A review of drivers and indicators at various scales. *Geoderma*, *333*, 149–162. https://doi.org/10.1016/j.geoderma.2018.07.026

Xiao, L., Wang, G., Wang, M., Zhang, S., Sierra, C. A., Guo, X., Chang, J., Shi, Z., & Luo, Z. (2022). Younger carbon dominates global soil carbon efflux. *Global Change Biology*, *28*(18), 5587–5599. https://doi.org/10.1111/gcb.16311

Yu, W., Weintraub, S. R., & Hall, S. J. (2021). Climatic and geochemical controls on soil carbon at the continental scale: Interactions and thresholds. *Global Biogeochemical Cycles*, *35*(3), e2020GB006781. https://doi.org/10.1029/2020GB006781

Zomer, R. J., Xu, J., & Trabucco, A. (2022). Version 3 of the global aridity index and potential evapotranspiration database. *Scientific Data*, *9*(1), 409. https://doi.org/10.1038/s41597-022-01493-1

SUPPORTING INFORMATION

Additional supporting information can be found online in the Supporting Information section at the end of this article.

How to cite this article: von Fromm, S. F., Hoyt, A. M., Sierra, C. A., Georgiou, K., Doetterl, S., & Trumbore, S. E. (2024). Controls and relationships of soil organic carbon abundance and persistence vary across pedo-climatic regions. *Global Change Biology*, *30*, e17320. https://doi.org/10.1111/gcb.17320